SLAC – PUB – 3937
April 1986
(M)

PHENOMENOLOGY OF THE MESON-SKYRMION SYSTEM*

MICHAEL P. MATTIS
Stanford Linear Accelerator Center
Stanford University, Stanford, California 94305

1. Introduction

This chapter is devoted to a study of meson-nucleon scattering in chiral soliton models of the nucleon.[1-3] Of course, scattering processes can be analyzed in several different energy regimes, each of which dictates its own set of appropriate approximations. The "soft-pion" limit, in particular, has been thoroughly examined by Schnitzer.[4] Instead, we shall be focusing our attention on the characteristic energy-range of the baryon resonances, typically 1.5-2.5 GeV. This is well beyond the point where current-algebra (*i.e.*, soft-pion physics) is valid; nor is QCD, which becomes tractable only when the momentum transfer is large, of any use. Thus it is especially interesting to see what insights emerge in this regime from skyrmion physics.

The meson-skyrmion system has been explored in a variety of interesting ways.[4-6] The particular approach that I shall follow was developed in collaboration with Marek Karliner and Michael Peskin at SLAC,[7-13] and independently by the group at Siegen University;[14-15] the prospective worker in the field is referred inevitably to the original references for full details.

The object of our investigations will be effective Lagrangians (Skyrme's included) of the form

$$\mathcal{L}_\pi = \frac{f_\pi^2}{16}\,\mathrm{Tr}\,(\partial_\mu U \partial^\mu U^\dagger) + \cdots . \tag{1}$$

The leading term is the usual 2-flavor or 3-flavor nonlinear sigma model, depending on whether $U \in SU(2)$ or $U \in SU(3)$. The dots stand for higher-derivative

* Work supported by the Department of Energy, contract DE-AC03-76SF00515.

To appear in CHIRAL SOLITONS, ed. K. F. Liu
World Scientific Press

terms, which are not usually exploited in traditional soft-pion physics, but are needed to stabilize a soliton. The standard identification of the pion field in (1) in the baryon-number-0 sector of the 2-flavor theory is via:

$$U(x) = \exp\left(\frac{2i}{f_\pi}\vec{\pi}(x)\cdot\vec{\sigma}\right). \tag{2}$$

Thus the pions can be thought of as "small fluctuations" about the trivial vacuum $U(x) \equiv 1$.

It is a straightforward procedure to introduce additional fields into (1) in such a way as to preserve chiral invariance.[16] In particular, the traditional (*i.e.*, post-Skyrme but pre-Witten) approach to studying the coupling of pions to the nucleon isodoublet N is to set

$$\mathcal{L}_{\pi N} = \frac{f_\pi^2}{16}\,\mathrm{Tr}\,(\partial_\mu U \partial^\mu U^\dagger) + \bar{N}(i\gamma^\mu \mathcal{D}_\mu - m)N + g_A \mathcal{D}_\mu\vec{\pi}\cdot\bar{N}\vec{\tau}\gamma^\mu\gamma^5 N. \tag{3}$$

Here $\mathcal{D}$ is the covariant derivative appropriate to the nonlinear sigma model with variables in the manifold

$$\frac{SU(2)_L \times SU(2)_R}{SU(2)_{\text{isospin}}}.$$

From this Lagrangian, all soft-pion theorems pertaining to the πN interaction, such as Weinberg's calculation of the S-wave scattering lengths,[17] can be derived.

It is the moral of this chapter that, insofar as the πN system is concerned, the purely mesonic Lagrangian (1) contains *at least* as much information as does (3)! Not only does (1) properly encompass soft-pion physics, as Schnitzer has shown,[4] but in addition—well beyond the soft-pion regime—it yields surprisingly accurate predictions concerning the spectrum of nucleon and Δ resonances and the qualitative behavior of the large majority of πN partial-wave amplitudes.

I will be reporting two different kinds of results. *Model-dependent* results depend on the particular form of the omitted terms indicated by dots in our starting Lagrangian, Eq. (1); in this review, the focus will be on the Skyrme Lagrangian in both its 2- and 3-flavor versions. *Model-independent* results, in contrast, are insensitive to the details of the Lagrangian; they thus serve as direct tests of both the treatment of the nucleon as a "hedgehog" soliton and of the $1/N$ expansion. The emphasis throughout will be on a detailed comparison with experiment.

The organization is as follows:[†] Section 2 spells out our various approximations, all of which fall under the rubric of "large N." Section 3 develops the group-theoretic formalism for πN scattering for any model in which the nucleon is regarded as a "hedgehog" soliton in the field of pions. It turns out that this formalism implies the existence of energy-independent linear relations for the $\pi N \to \pi N$ and $\pi N \to \pi \Delta$ partial-wave amplitudes; these relations are tested on the experimental scattering data in Section 4.

Section 5 applies the formalism of Section 3 to the particular case of the Skyrme Lagrangian. The spectrum of nucleon and Δ resonances of the model is calculated from a phase-shift analysis; the masses obtained turn out to be accurate on the average to 8% of their experimental values up to 3 GeV. For most channels, the model reproduces many significant features of the experimental $\pi N \to \pi N$ and $\pi N \to \pi \Delta$ Argand diagrams correctly, although there are severe discrepancies in some of the low partial waves.

In Section 6 we discuss a strikingly consistent pattern, which we have dubbed the "big-small-small-big" pattern, characterizing the four independent $\pi N \to \pi N$ amplitudes for each value of pion angular momentum in both the Skyrme model and in Nature. It is shown that the chiral soliton approach provides a natural framework for understanding this effect.

Finally, Sections 7-9 discuss two orthogonal extensions of the formalism, first to the case in which the incoming and/or outgoing meson has spin, and then to the case of three light flavors. This enables us to broaden the scope of our study to include a host of experimentally-measured processes such as $\pi N \to \rho N$ and $\overline{K} N \to \pi \Sigma$, with a reasonable degree of success.

2. Large N

Most of the approximations we will make relate in one way or another to the large-N expansion, which many consider the *raison-d'être* of skyrmion physics. In general, the results presented in the forthcoming Sections will only be valid to *leading order* in $1/N$.

Our major approximation will be that of deriving the meson-nucleon amplitudes from the lowest-order meson propagator in the (appropriately rotated) soliton background, ignoring all loop contributions to the two-point function. Loop diagrams necessarily contain 3-meson, 4-meson or higher-order vertices which are damped by increasingly higher powers of $f_\pi^{-1} \sim N^{-\frac{1}{2}}$. Consequently,

† The material in Sections 2-4 is largely drawn from Ref. 8; Section 5, from Refs. 7 and 13; Section 7, from Refs. 8 and 13; Section 7, from Ref. 10; Section 8, from Refs. 11-13; and Section 9, from Refs. 12 and 13.

all loop contributions to the propagator are suppressed by at least one power of N and can therefore be disregarded in our lowest-order treatment. The resulting Euler-Lagrange equations of motion for the meson field will be *linear* (in agreement with Witten's result obtained from counting quark-gluon diagrams in large-N QCD[18]).

Another limitation of our lowest-order large-N analysis is that it is appropriate only to 2-body scattering. Multiple pion production, for instance, is formally suppressed by powers of $1/\sqrt{N}$;[19] nevertheless, in Nature it becomes the dominant feature of πN collisions at high energies.

The fact that the bare meson propagator has enough structure to lead to nontrivial scattering is noteworthy and deserves some comment. On the one hand, this should be expected from the soliton picture, since meson-soliton scattering normally appears at zeroth order in a weak-coupling expansion.[18] On the other hand, this fact implies that, in large N, baryon resonances are not at all the counterparts of excited mesons. As is well known,[19] the widths of all excited mesons vanish like N^{-1} as $N \to \infty$. Among the baryons found in Nature, however, only the nucleon and Δ (and perhaps a handful of others: see Section 5) appear as sharply defined states in this limit. Higher-mass baryons cannot be identified with narrow states; they appear only as resonances above threshold in the various channels of pion-nucleon scattering. The widths of these baryons are determined by the motion of the meson-nucleon phase shifts in the relevant partial waves; since the equations that determine these phase shifts have a definite, finite large-N limit, both the widths and the excitation energies of these resonances will be of order N^0.

This picture contrasts sharply with the quark model description of baryon resonances. One may think of the quark model as representing the leading term in a nonrelativistic approximation to the baryon and meson states. In this limit, unlike that of large N, the baryon resonances appear as eigenstates of a Hamiltonian and hence are *stable* to lowest order.

Our second approximation will consist of ignoring the rotation of the soliton during the scattering process. As explained by Adkins, Nappi and Witten,[3] nucleons and Δ's correspond in the chiral soliton models to *rotating* hedgehog solitons of angular momentum $\mathbf{J}^2 = s(s+1)$, with $s = \frac{1}{2}$ and $s = \frac{3}{2}$, respectively (Fig. 1). The nucleon-Δ mass difference is then simply due to the rotational kinetic energy term $\mathbf{J}^2/2I$, where I denotes the moment of inertia of the soliton. Since $I \sim N$ this mass splitting is a $1/N$ effect. (For example, in the Skyrme model,[3]

$$m_{N,\Delta} \cong 36.5\frac{f_\pi}{e} + \frac{s(s+1)}{2I}, \quad I \cong \frac{106}{e^3 f_\pi}, \tag{4}$$

where, in the large-N limit, $e \sim N^{-\frac{1}{2}}$ and $f_\pi \sim N^{\frac{1}{2}}$ in order that the Skyrme Lagrangian scale like N.) The rotational frequency of the soliton is then given by $\omega = J/I$, which likewise vanishes like $1/N$ for large N, thereby justifying our approximation in this limit.

5-85 5395A1

Fig. 1. A rotating hedgehog.

This argument might not appear particularly compelling when applied to the real world, where $N = 3$. However one can reverse the above relations and solve for ω in terms of m_N and m_Δ; the result is $\omega = \frac{2}{3}J(m_\Delta - m_N)$. The ratio of the time it takes a meson of velocity v to cross the charge radius R of a nucleon to the period of rotation of the nucleon viewed as a soliton is then $(v/c)^{-1}(\omega R/2\pi)$ $\approx \frac{1}{16}(v/c)^{-1}$, while the corresponding ratio in the case of the Δ is roughly $\frac{1}{5}(v/c)^{-1}$. Thus, for example, our approximation appears to be a reasonable one for $\pi N \to \pi N$ so long as $v/c \approx 1$, whereas for $\pi N \to \pi\Delta$ it is somewhat more severe. Note that this approximation *breaks down* near threshold, where $v/c \to 0$. In this regime, it is Schnitzer's "soft-pion" approach, instead, that becomes appropriate.[4]

Finally, we will ignore both the deformation and the recoil of the soliton. This, too, can be formally justified for large N, since in this limit the baryon (which is made of N quarks) is much more massive than the meson (which can always be thought of as a quark-antiquark pair).

In sum, our various approximations pick out an *intermediate energy regime* which is, on the one hand, sufficiently past the soft-pion limit that we can neglect the rotation of the skyrmion during the scattering process, and on the other

hand, low enough that we can ignore both baryon recoil and multiple meson production. Admittedly, it is not clear *a priori* that such a regime exists! But luckily judging from the results, it not only exists, but in fact seems to encompass practically the entire energy range of the baryon resonances.

In the next four Sections, we shall specialize to the processes $\pi N \to \pi N$ and $\pi N \to \pi \Delta$. These are the easiest meson-baryon processes to analyze in the chiral soliton approach. And fortunately, the experimental situation in both cases is excellent. Thus they constitute particularly rigorous proving-grounds for skyrmion physics.

3. Outline of Formalism

We begin our analysis of πN scattering from Skyrme's assumption that the solitons associated with the Lagrangian (1) have the hedgehog form:

$$U_\circ(\vec{x}) = \exp(iF(r)\hat{\mathbf{r}} \cdot \vec{\sigma}). \tag{5}$$

When $F(r)$ tends to 0 as $r \to \infty$ and to π as $r \to 0$, this defines a configuration with topological charge equal to unity—a skyrmion. This configuration is maximally symmetric in the sense that, although it is not invariant with respect to isospin or spatial rotations separately, it is invariant under a combination of space and isospace rotations. We shall refer to (5) as a hedgehog skyrmion in its canonical (*i.e.*, unrotated) orientation (Fig. 2).

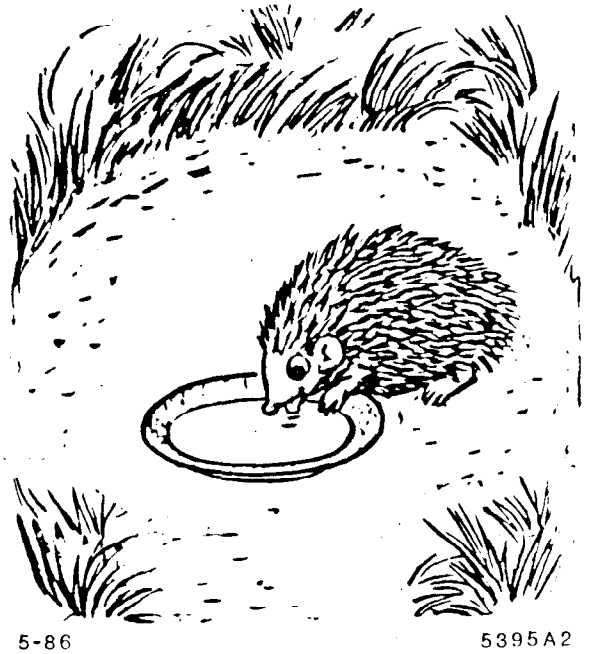

5-86 5395A2

Fig. 2. An unrotated hedgehog.

Of course, $U_\circ$ as it stands is not a suitable candidate for a nucleon or Δ; this is because physical baryons are characterized by definite values of spin and isospin *individually*. One obtains a state with the correct quantum numbers by introducing "collective coordinates" $A(t) \in SU(2)$, which rotate the skyrmion as in Eq. (12) below, and by assigning the baryon an appropriately chosen wavefunction $\chi(A)$.* Nevertheless, for convenience, let us forget about the collective coordinate structure of the nucleon for the moment, and concentrate instead on the simplified problem of a pion scattering from an unrotated skyrmion.

In analogy to Eq. (2), we can represent pion fields in the baryon-number-1 sector of the theory as "small fluctuations" about the classical soliton by letting

$$F(r)\hat{\mathbf{r}} \to F(r)\hat{\mathbf{r}} + \frac{2}{f_\pi}\vec{\pi}(\vec{x},t) \tag{6}$$

in the exponent of (5). Plugging this "new improved" $U(x)$ into Eq. (1) and expanding about the skyrmion in powers of the pion field yields an action of the form:

$$S = -\int dt\, m_\circ + \int d^4x\, \pi^{i*}(x)\widehat{\mathbf{L}}_{ij}\pi^j(x) + \mathcal{O}(\pi^3/f_\pi), \tag{7}$$

where $m_\circ$ is the mass of the soliton and i and j are isospin indices. $\widehat{\mathbf{L}}$ is accordingly a 3×3 matrix of differential operators formed from various products of $\partial_i, \partial_t^2, \hat{r}_i, \delta_{ij}$ and ϵ_{ijk}. That is,

$$\widehat{\mathbf{L}}_{ij} = G_1(r)\delta_{ij} + G_2(r)\delta_{ij}\partial_t^2 + G_3(r)\hat{r}_i\hat{r}_j\partial_t^2 + G_4(r)\,\hat{r}_j\partial_i + G_5(r)\hat{r}_i\partial_j + \cdots \tag{8}$$

with the G_k's being, in general, horrible, model-dependent functions of the soliton profile $F(r)$ and its derivatives. We note that, with no loss of generality, $\widehat{\mathbf{L}}$ can be chosen uniquely to be self-adjoint. As discussed in Section 2, we shall henceforth neglect all $\mathcal{O}(\pi^3/f_\pi)$ terms in keeping with our lowest-order approach.

Complicated though $\widehat{\mathbf{L}}$ may be, it respects the "hybrid" symmetry

$$\mathbf{K} \equiv \mathbf{I}(pion) + \mathbf{L}(pion). \tag{9}$$

Explicitly,

$$\left(-i\epsilon_{ijk}r^i\partial_j\delta_{bc} + i\epsilon_{kbc}\right)\widehat{\mathbf{L}}_{ba} - \widehat{\mathbf{L}}_{cb}\left(-i\epsilon_{ijk}r^i\partial_j\delta_{ba} - i\epsilon_{kba}\right) = 0. \tag{10}$$

Consequently $\widehat{\mathbf{L}}$ preserves the subspaces of pion states of definite $\mathbf{K}^2$ and K_z.

---

* I shall assume familiarity with the method of collective coordinates; see Ref. 3 for details.

This peculiar symmetry property of $\hat{\mathbf{L}}$, which follows purely from the hedgehog form of the skyrmion, greatly simplifies the otherwise formidable task of constructing the propagator

$$\left\langle \pi^i(x')\pi^j(x) \right\rangle_\circ$$

of the pion field in the skyrmion background. (The "nought" on the propagator serves to remind us that the skyrmion is in its canonical orientation, Eq. (5).) The smart thing to do, of course, is to project the pion onto a complete set of states of definite $\mathbf{K}^2$ and K_z. This is best accomplished as follows: First, the initial and final pion fields are expanded in spherical harmonics $|LM>$ and $|L'M'>$, respectively. Orbital angular momentum is then added to the pions' isospin to form states $|\mathbf{K}^2 K_z L>$ and $|\mathbf{K}'^2 K'_z L'>$. The K-symmetry of $\hat{\mathbf{L}}$ then guarantees that $\mathbf{K}^2 = \mathbf{K}'^2$ and $K_z = K'_z$. In equations:

$$\left\langle \pi^m(\vec{x}',t')\pi^{n*}(\vec{x},t) \right\rangle_\circ = \sum_{LML'M'} \left\{ Y_{L'M'}(\Omega')Y^*_{LM}(\Omega) \times \right.$$
$$\left. \sum_{KK_z} \langle KK_z|L1Mn\rangle \, \langle L'1M'm|KK_z\rangle \, \mathcal{T}_{KL'L}(rt;r't') \right\}. \tag{11}$$

Here, the quantity $\mathcal{T}_{KL'L}$ is the "reduced" amplitude characterizing the scattering process; it carries all the detailed model-independent dynamical information contained in our starting effective Lagrangian, Eq. (1). For each value of K, $\mathcal{T}_K$ can be thought of as a unitary 3×3 matrix, with "row" and "column" indices L' and L ranging from $K-1$ to $K+1$. Parity requires that $\mathcal{T}_{KL'L} = 0$ when $|L - L'| = 1$. Furthermore, by time-reversal invariance and unitarity, $\mathcal{T}_K$ can be shown to be symmetric:[7-8]

$$\mathcal{T}_{KL'L} = \mathcal{T}_{KLL'}.$$

Apart from these constraints, $\mathcal{T}_K$ must be determined by a detailed, model-dependent phase-shift analysis, as illustrated in Section 5 below for the special case of the Skyrme model.

For future reference, we should note that not all pion fluctuations of the form (6) should be identified with *bona fide* mesonic degrees of freedom. In particular, we can find $\vec{\pi}$'s that serve only to rotate or translate the skyrmion, and which should therefore be viewed as *baryonic* degrees of freedom. Since such fluctuations do not change the energy of the system, they occur at zero frequency ($\omega = 0$). It turns out that:

(i) the rotational zero-modes manifest themselves as threshold poles in the reduced amplitude $\mathcal{T}_{111}$, and

(ii) the translational zero-modes show up as threshold poles in $\mathcal{T}_{100}$, $\mathcal{T}_{122}$, and $\mathcal{T}_{102}$.

We shall make use of these facts in Sections 4 and 5.

So far, we have focused, not on physical πN or $\pi\Delta$ processes *per se*, but rather on the simplified problem of a pion scattering from an unrotated hedgehog. Physical scattering requires that we restore the skyrmion's collective coordinates. As an intermediate step in this direction, it is straightforward to generalize Eq. (11) to the case when the pion scatters, not from U_0, but rather from a "tilted" skyrmion U_A, defined by*

$$U_A = \mathcal{D}^{\frac{1}{2}}(A) U_0 \mathcal{D}^{\frac{1}{2}}(A)^{-1} = \exp\{iF(r)(\mathcal{D}^1(A)\hat{\mathbf{r}}) \cdot \vec{\sigma}\}. \tag{12}$$

Pion fluctuations can be naturally incorporated into U_A by letting

$$F(r)\mathcal{D}^1(A)\hat{\mathbf{r}} \to F(r)\mathcal{D}^1(A)\hat{\mathbf{r}} + \frac{2}{f_\pi}\vec{\pi}(\vec{x},t)$$

as before.† This results in

$$\left\langle \pi^i \pi^j \right\rangle_\circ \to \left\langle \pi^i \pi^j \right\rangle_A = \mathcal{D}^1(A)_{im} \left\langle \pi^m \pi^n \right\rangle_\circ \mathcal{D}^1(A)^{-1}_{nj}. \tag{13}$$

It is now a simple matter to express the Green's functions for the physical processes $\pi N \to \pi N$, $\pi N \to \pi\Delta$ and $\pi\Delta \to \pi\Delta$. As discussed in Section 2, we shall assume that the scattering event happens quickly enough that the baryon does not rotate appreciably in the interim. This is equivalent to saying that the pion only sees a *fixed* value of the baryon's collective coordinate A in the process. Of course, we are doing quantum mechanics, so we ultimately have to perform a superposition over all possible A's, weighted by the initial and final baryon wavefunctions* $\chi^s_{i_z s_z}(A)$ and $\chi^{s'}_{i'_z s'_z}(A)$, respectively. Thus the physical

---

* Here, $\mathcal{D}^{\frac{1}{2}}(A)$ and $\mathcal{D}^1(A)$ represent the spin-$\frac{1}{2}$ and spin-1 representations of the $SU(2)$ collective coordinate A.

† For calculating on-shell amplitudes, this parametrization of the meson fields is equivalent to the one advocated by Schnitzer.[4]

* Here s is the spin of the baryon, *i.e.*, $\frac{1}{2}$ for nucleons and $\frac{3}{2}$ for Δ's; s_z and i_z are the z-components of the baryon's spin and isospin, respectively.

Green's functions are given by

$$\left\langle \pi^i \pi^j \right\rangle_{\text{physical}} = \int\limits_{SU(2)} dA \; \chi^{s'}_{i'_z s'_z}(A)^* \left\langle \pi^i \pi^j \right\rangle_A \chi^{s}_{i_z s_z}(A)$$

$$= \int\limits_{SU(2)} dA \; \chi^{s'}_{i'_z s'_z}(A)^* D^1(A)_{im} \langle \pi^m \pi^n \rangle_\circ \, D^1(A)^{-1}_{nj} \chi^{s}_{i_z s_z}(A). \tag{14}$$

It turns out that the A-integration in Eq. (14) can be carried out in closed form, thanks to the convenient expression for the nucleon and Δ wavefunctions‡

$$\chi^{s}_{i_z s_z}(A) = \frac{i}{\pi} \sqrt{\tfrac{1}{2}(2s+1)} \left(\epsilon^s D^s(A)^\dagger \right)_{s_z i_z} \tag{15}$$

and to the identities

$$\begin{aligned} D^{s_1}(A)_{ab} D^{s_2}(A)_{cd} = \sum_{\tilde{s}} D^{\tilde{s}}(A)_{a+c,b+d} \quad \times \\ < s_1 s_2 ac | \tilde{s}, a+c, s_1 s_2 > < \tilde{s}, b+d, s_1 s_2 | s_1 s_2 bd > \end{aligned} \tag{16}$$

and

$$\int dA \, D^{s_1}(A)_{ab} D^{s_2}(A)^\dagger_{cd} = \frac{2\pi^2}{2s_1+1} \delta_{s_1 s_2} \delta_{bc} \delta_{ad}. \tag{17}$$

This eliminates all explicit dependence on the collective coordinates.

Thanks to Eqs. (11)-(17), we have succeeded in constructing an explicit (if somewhat unwieldy) expression for $< \pi^i \pi^j >_{\text{physical}}$ in terms of (i) spherical harmonics, (ii) reduced amplitudes $\mathcal{T}_{KL'L}$, and (iii) a large number of Clebsch-Gordan coefficients. Fortunately, this expression greatly simplifies if one projects (more Clebsches!) the initial and final pion-baryon states onto states of definite total isospin and angular momentum $|II_zJJ_z\rangle$ and $|I'I'_zJ'J'_z\rangle$. ($\vec{I}$ and $\vec{J}$ will of course turn out to be conserved in the scattering process.) For, as we shall see in a moment, the Clebsches then collapse neatly into a product of two $6j$ symbols and four Kronecker δ's. Our final formula can be stated in the most compact way if, in addition, we restrict the incoming and outgoing pions to orbital angular

‡ Note that these wavefunctions are really only appropriate for baryons at rest; however, as we have discussed in Section 2, we plan in any event to neglect the baryon's recoil in the scattering process. ϵ^s in Eq. (15) denotes the antisymmetric tensor in the spin-s representation.

momenta L and L', respectively. The resulting pion Green's functions, which we label $\mathbf{T}_{LL'ss'IJ}(rt;r't')$, are then given by:[♮]

$$\mathbf{T}_{LL'ss'IJ}(rt;r't') = \delta_{II'}\delta_{I_zI'_z}\delta_{JJ'}\delta_{J_zJ'_z} \quad \times$$
$$\sum_K (-1)^{s'-s}\sqrt{(2s+1)(2s'+1)}(2K+1)\begin{Bmatrix} KIJ \\ s'L'1 \end{Bmatrix}\begin{Bmatrix} KIJ \\ sL1 \end{Bmatrix} \cdot \mathcal{T}_{KL'L}(rt;r't'). \tag{18}$$

This is the main result of this Section.

Note that conservation of total isospin and angular momentum has manifested itself in the Kronecker δ's. The appearance of $6j$-symbols in this expression is also quite natural, since, as indicated in Fig. 3, the problem in both the entering and the exiting πN or $\pi\Delta$ channels is characterized by six intertwined angular momenta. Each face of the tetrahedron can be read as a triangle inequality among the quantities that enter into Eq. (18); together, the "entering" and "exiting" tetrahedra thus furnish seven independent triangle inequalities (since the $\{KIJ\}$ face is common to both). It nevertheless turns out that (18) imposes *no unphysical selection rules* on the scattering process, in other words, nothing apart from the usual conservation of isospin, angular momentum, and parity. In particular, the quantum number $\mathbf{K}$, which is conserved when a pion scatters from an *unrotated* hedgehog, is no longer conserved in scattering from a *rotating* skyrmion such as a nucleon or Δ.

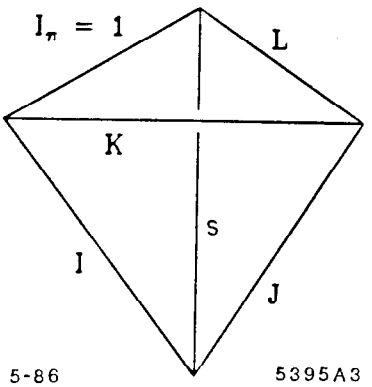

Fig. 3 (from Ref. 8). Relation of the six coupled angular momenta in either the initial or the final state of pion-skyrmion scattering.

[♮] Explicit formulas for the group-theoretic coefficients in Eq. (18) relevant to $\pi N \to \pi N$ and $\pi N \to \pi\Delta$ are presented in Appendix B of Ref. 8.

Note that all the model dependence in (18) arising from the details of the Lagrangian (1) is subsumed in the reduced amplitudes $\mathcal{T}_{KL'L}$; the $6j$-symbols, in contrast, follow purely from the assumed hedgehog nature of the chiral soliton. Equation (18) is thus analogous to the Wigner-Eckart theorem in that a large number of physical matrix elements (the $\mathbf{T}$'s) are expressed in terms of a substantially smaller set of reduced matrix elements (the $\mathcal{T}_K$'s) weighted by appropriate group-theoretical coefficients. One can carry the analogy further by finding those special linear combinations (analogous to the Gell-Mann-Okubo formula) for which the model-dependent right-hand side of (18) cancels out; the net result will be a set of energy-independent linear relations between physical scattering amplitudes that serve as a test of the applicability of skyrmion physics to the real world. This program is carried out in Section 4. Alternatively, one can calculate the $\mathcal{T}_K$'s numerically in the framework of a specific model such as Skyrme's, reconstruct the complete partial-wave S-matrix, and then compare with experiment; this is the approach of Section 5.

4. Model-independent linear relations for $\pi N \to \pi N$ and $\pi N \to \pi\Delta$

In this Section we apply Eq. (18) directly to the *experimental* $\pi N \to \pi N$ and $\pi N \to \pi\Delta$ partial-wave amplitudes. Consider the elastic case first. In the notation of Eq. (18), this corresponds to the physical amplitude $\mathbf{T}_{LL\frac{1}{2}\frac{1}{2}IJ}$, which we shall henceforth express more descriptively as* $\mathbf{T}^{\pi N\pi N}_{LIJ}$.

Let us pause to see why, on general grounds, model-independent relations between the $\mathbf{T}$'s can be expected to emerge from the chiral soliton framework. For each value of pion angular momentum L, there are four independent $\pi N \to \pi N$ amplitudes, corresponding to total isospin $I = \{\frac{1}{2}, \frac{3}{2}\}$ and total angular momentum $J = L \pm \frac{1}{2}$. With the help of (18), these four $\mathbf{T}$'s can be expressed as linear combinations of only *three* reduced amplitudes $\mathcal{T}_{KLL}$, with $K = \{L-1, L, L+1\}$. Specifically, using explicit formulae for $6j$ symbols,† one finds:

$$\mathbf{T}^{\pi N\pi N}_{L\frac{1}{2},L-\frac{1}{2}} = \frac{2L-1}{3L} \cdot \mathcal{T}_{L-1,LL} + \frac{L+1}{3L} \cdot \mathcal{T}_{LLL}, \tag{19a}$$

$$\mathbf{T}^{\pi N\pi N}_{L\frac{1}{2},L+\frac{1}{2}} = \frac{L}{3L+3} \cdot \mathcal{T}_{LLL} + \frac{2L+3}{3L+3} \cdot \mathcal{T}_{L+1,LL}, \tag{19b}$$

---

* In order to facilitate comparison to experiment, we will present all our results in terms of T-matrix elements. The T-matrix is related to the S-matrix via $\mathbf{T} = (\mathbf{S} - \mathbf{1})/2i$, where $\mathbf{1}$ is the identity operator on the Hilbert space (which vanishes for inelastic scattering).

† See Appendix B of Ref. 8.

$$\mathbf{T}^{\pi N\pi N}_{L\frac{3}{2},L-\frac{1}{2}} = \frac{(2L-1)(L-1)}{6L(2L+1)}\cdot\tau_{L-1,LL} + \frac{2L-1}{6L}\cdot\tau_{LLL} + \frac{2L+3}{4L+2}\cdot\tau_{L+1,LL}, \tag{19c}$$

$$\mathbf{T}^{\pi N\pi N}_{L\frac{3}{2},L+\frac{1}{2}} = \frac{2L-1}{4L+2}\cdot\tau_{L-1,LL} + \frac{2L+3}{6L+6}\cdot\tau_{LLL} + \frac{(L+2)(2L+3)}{(6L+6)(2L+1)}\cdot\tau_{L+1,LL}. \tag{19d}$$

We are thus assured of the existence of *at least one* nontrivial linear relation between the $\mathbf{T}$'s for each value of L for which the (model-dependent) right-hand sides of (19) cancel out.

As it turns out, there are *two* such relations for each L, which we can use (for example) to solve for the isospin-$\frac{3}{2}$ amplitudes in terms of the isospin-$\frac{1}{2}$ amplitudes. One easily finds:

$$\mathbf{T}^{\pi N\pi N}_{L\frac{3}{2},L-\frac{1}{2}} = \frac{L-1}{4L+2}\cdot\mathbf{T}^{\pi N\pi N}_{L\frac{1}{2},L-\frac{1}{2}} + \frac{3L+3}{4L+2}\cdot\mathbf{T}^{\pi N\pi N}_{L\frac{1}{2},L+\frac{1}{2}} \tag{20a}$$

and

$$\mathbf{T}^{\pi N\pi N}_{L\frac{3}{2},L+\frac{1}{2}} = \frac{3L}{4L+2}\cdot\mathbf{T}^{\pi N\pi N}_{L\frac{1}{2},L-\frac{1}{2}} + \frac{L+2}{4L+2}\cdot\mathbf{T}^{\pi N\pi N}_{L\frac{1}{2},L+\frac{1}{2}}. \tag{20b}$$

Similar relations can be derived for $\pi N \to \pi\Delta$. In this case we can have either $L = L'$ or $L = L' \pm 2$ consistent with angular momentum conservation. For $L = L'$ we find:*

$$\mathbf{T}^{\pi N\pi\Delta}_{LL\frac{3}{2},L-\frac{1}{2}} = \frac{4(L-1)}{\sqrt{10}(2L+1)}\cdot\mathbf{T}^{\pi N\pi\Delta}_{LL\frac{1}{2},L-\frac{1}{2}} + \frac{3}{2L+1}\sqrt{\frac{(L+1)(2L+3)(2L-1)}{10L}}\cdot\mathbf{T}^{\pi N\pi\Delta}_{LL\frac{1}{2},L+\frac{1}{2}} \tag{21a}$$

and likewise

$$\mathbf{T}^{\pi N\pi\Delta}_{LL\frac{3}{2},L+\frac{1}{2}} = \frac{3}{2L+1}\sqrt{\frac{L(2L+3)(2L-1)}{10(L+1)}}\cdot\mathbf{T}^{\pi N\pi\Delta}_{LL\frac{1}{2},L-\frac{1}{2}} + \frac{4(L+2)}{\sqrt{10}(2L+1)}\cdot\mathbf{T}^{\pi N\pi\Delta}_{LL\frac{1}{2},L+\frac{1}{2}}, \tag{21b}$$

* We are rewriting $\mathbf{T}_{LL'\frac{1}{2}\frac{3}{2}IJ}$ as $\mathbf{T}^{\pi N\pi\Delta}_{LL'IJ}$.

while for $L = L' \pm 2$ we obtain the simple proportionality relations

$$\begin{aligned}\sqrt{L+1}\cdot \mathbf{T}^{\pi N\pi\Delta}_{L,L+2,\frac{1}{2},L+\frac{1}{2}} &= -\sqrt{10(L+1)}\cdot \mathbf{T}^{\pi N\pi\Delta}_{L,L+2,\frac{3}{2},L+\frac{1}{2}} \\ &= -\sqrt{L+2}\cdot \mathbf{T}^{\pi N\pi\Delta}_{L+2,L\frac{1}{2},L+\frac{3}{2}} = \sqrt{10(L+2)}\cdot \mathbf{T}^{\pi N\pi\Delta}_{L+2,L\frac{3}{2},L+\frac{3}{2}}.\end{aligned} \tag{22}$$

Finally, for each L, one can derive an additional independent linear relation which serves to relate $\pi N \to \pi N$ to $\pi N \to \pi\Delta$:

$$\mathbf{T}^{\pi N\pi N}_{L\frac{1}{2},L-\frac{1}{2}} - \mathbf{T}^{\pi N\pi N}_{L\frac{1}{2},L+\frac{1}{2}} = \sqrt{\frac{2L-1}{L+1}}\cdot \mathbf{T}^{\pi N\pi\Delta}_{LL\frac{1}{2},L-\frac{1}{2}} + \sqrt{\frac{2L+3}{L}}\cdot \mathbf{T}^{\pi N\pi\Delta}_{LL\frac{1}{2},L+\frac{1}{2}}. \tag{23}$$

We turn now to an examination of how well these relations are obeyed in Nature.

Confronting Experiment: $\pi N \to \pi N$

Elastic πN scattering in the resonance region has been the subject of thorough experimental investigation. Our analysis in this Section relies on the data compilation of Höhler, *et al.*,[20] in which a complete partial-wave analysis of elastic πN scattering is presented for center-of-mass energies W up to 4.5 GeV. For elastic scattering the relevant linear relations are given by Eq. (20), which expresses the two isospin-$\frac{3}{2}$ amplitudes as linear combinations of the two isospin-$\frac{1}{2}$ amplitudes with the same L. We now examine the experimental validity of these relations.

In Fig. 4, we display the experimental isospin-$\frac{3}{2}$ πN scattering amplitudes for $L \leq 7$ juxtaposed with those particular linear combinations of isospin-$\frac{1}{2}$ amplitudes to which they are predicted to correspond; these are indicated by solid and dashed lines, respectively.‡ The closeness of these comparisons can be considered a model-independent test, not only of the chiral-soliton description of baryons, but also of the extent to which a lowest-order analysis in the $1/N$ expansion can be trusted to give a reasonable description of Nature.

The most striking feature of the graphs taken as a whole is the substantial qualitative agreement that one finds between "theory" and experiment, particularly for $L \geq 3$ (F-waves and higher). On a quantitative level, it turns out that, with few exceptions, the actual $I = \frac{3}{2}$ resonances are typically more massive by 150-300 MeV than predicted by the superposed $I = \frac{1}{2}$ amplitudes. This systematic splitting is presumably caused by the same rotational energy contribution

‡ πN channels are labeled $L_{2I,2J}$, where L is the pion's orbital angular momentum ($L = S, P, D, F, \ldots$), and I and J denote the total isospin and angular momentum of the πN system.

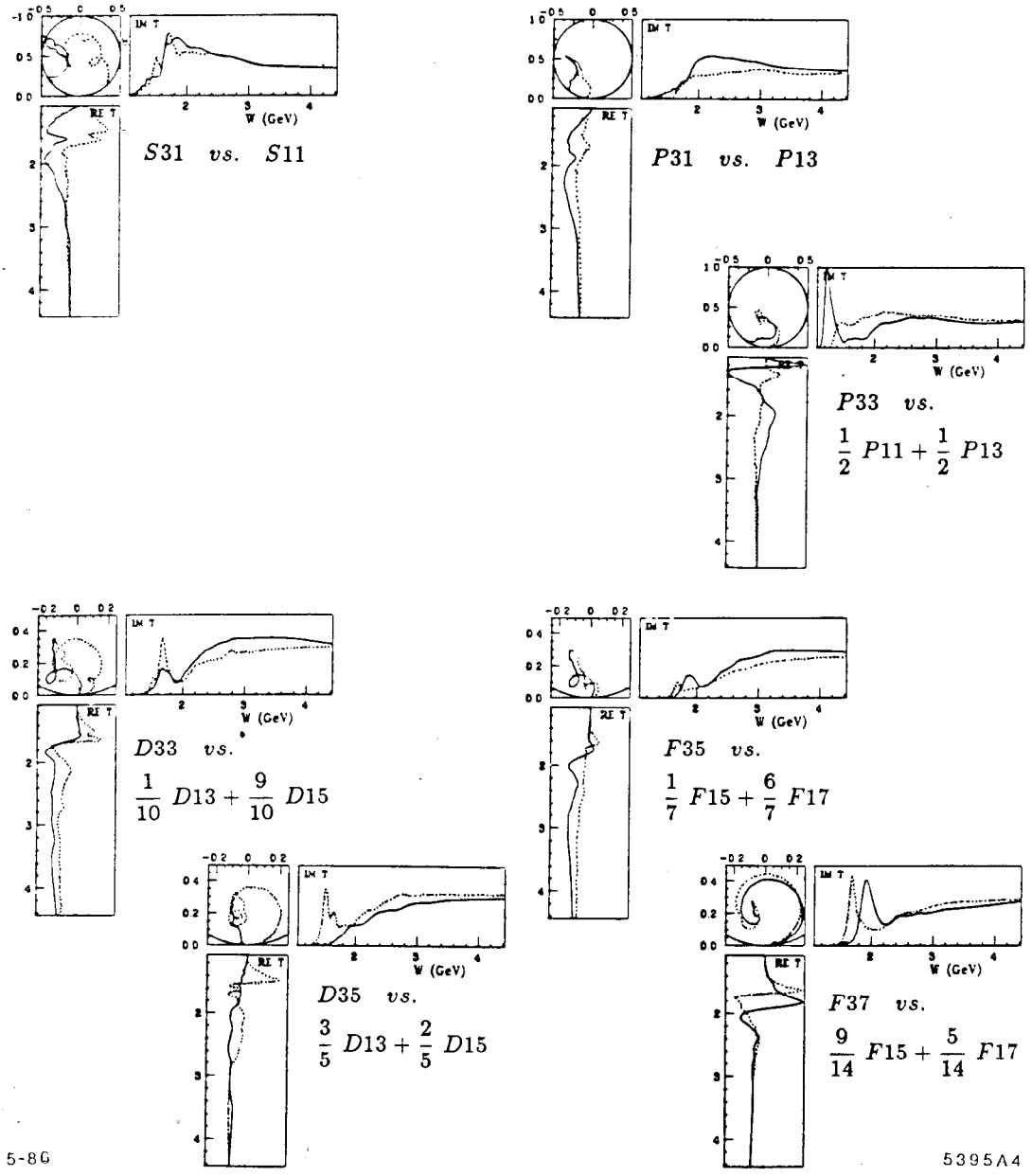

Fig. 4 (from Ref. 8). Experimentally determined $I = \frac{3}{2}$ partial-wave amplitudes for πN elastic scattering, plotted together with the linear combinations of $I = \frac{1}{2}$ amplitudes which should reproduce them if Eq. (20) is valid. The $I = \frac{3}{2}$ amplitudes are indicated by solid lines, the $I = \frac{1}{2}$ combinations by dotted lines. As is customary, we have plotted the real and imaginary parts of the partial-wave T-matrix, not only against each other, but also against c.o.m. energy.

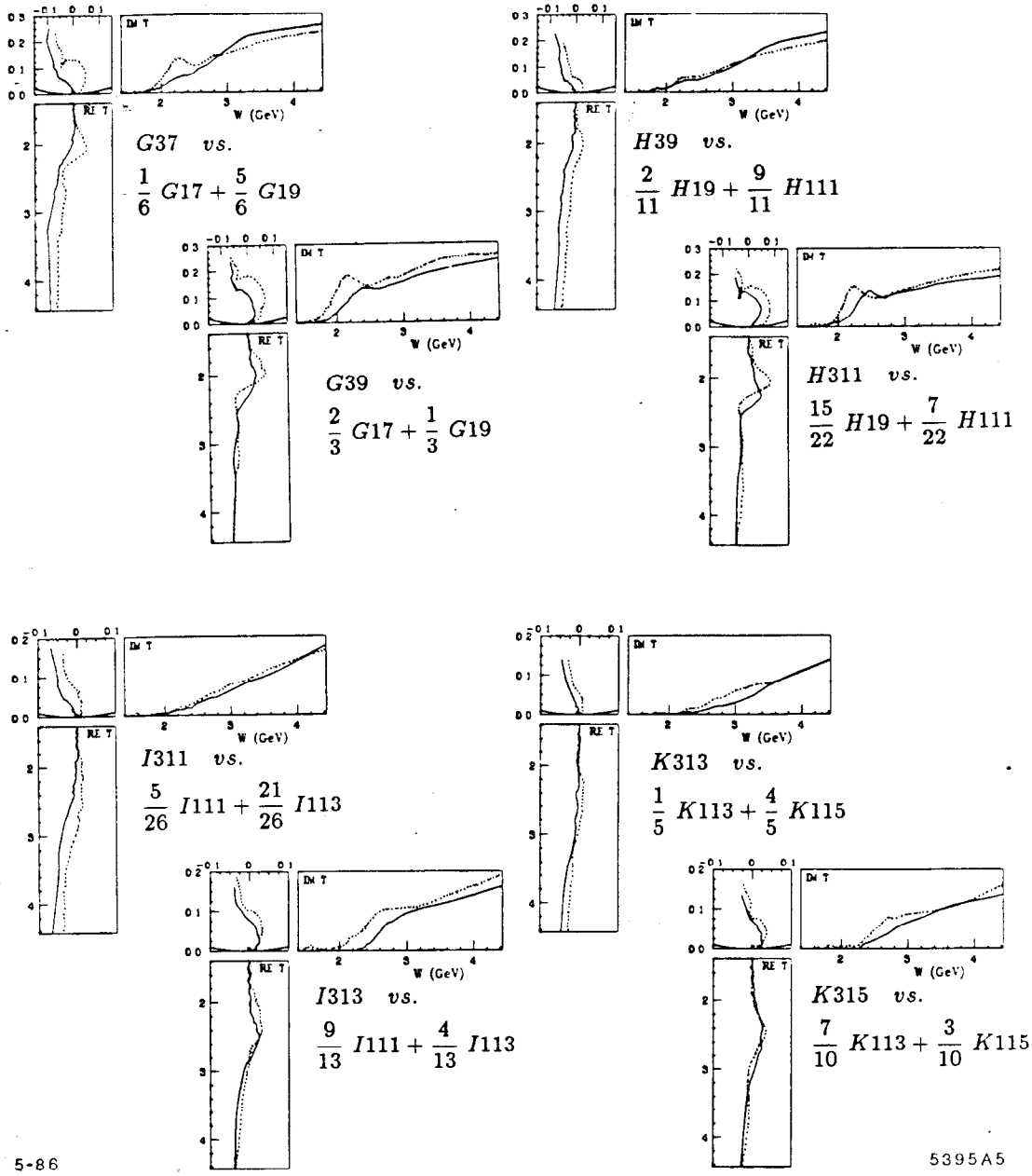

Fig. 4. Continued

that is responsible for the nucleon-Δ mass difference; since this is a $1/N$ effect, it does not, indeed cannot, emerge in our lowest-order analysis. In contrast, it is apparent on the whole that the *shapes* of the resonances are correctly predicted by Eq. (20), and that the form of the backgrounds are reproduced quite satisfactorily. The correlation between the detailed structure of the F_{37} resonance and the corresponding linear combination $\frac{9}{14}F_{15} + \frac{5}{14}F_{17}$ is particularly remarkable. Note that the background contributions tend to be given correctly even in those low-L channels such as P_{33} for which the structure of the resonances is not reproduced well.

Having noted the generally high degree of agreement, it is of course important to confront the disappointing results in the S_{31}, P_{33} and D_{35} channels. It turns out that the poor agreement in these channels is not necessarily fatal to the chiral soliton program. To see this, note that in each case the discrepancies are clearly the greatest near threshold. Now, it is a property of all chiral soliton models in which the soliton is of the hedgehog form that the threshold behavior of the S-, P- and D-wave amplitudes (and *only* these amplitudes) is extremely sensitive to small perturbations. (This point will be argued in Section 5.) The upshot is that it is completely unrealistic to expect a lowest-order calculation in $1/N$ such as ours to yield good agreement near threshold for the S-, P- and D-wave amplitudes. We find it encouraging that these are the only partial waves which are in serious disaccord with Eq. (20) at low energies, and furthermore, that at higher energies (albeit still in the resonance region) the agreement markedly improves.

Before leaving the discussion of discrepancies in the low-lying partial waves, we should address the subject of the apparent violation of Weinberg's well-known calculation[17] of the S-wave scattering-lengths* $a_{I=\frac{1}{2}}$ and $a_{I=\frac{3}{2}}$. The prediction is

$$a_{I=\frac{1}{2}} = -2a_{I=\frac{3}{2}} = \frac{g_V^2}{\pi f_\pi^2} \cdot \frac{m_\pi m_N}{m_\pi + m_N}, \tag{24}$$

which, in particular, correctly implies that the isospin-$\frac{1}{2}$ and isospin-$\frac{3}{2}$ S-wave amplitudes should exhibit attractive and repulsive behavior, respectively, near threshold. In contrast, the chiral-soliton prediction emerging from Eq. (20*b*) is that these amplitudes should be identically *equal* to one another:

$$a_{I=\frac{1}{2}} = a_{I=\frac{3}{2}}. \tag{25}$$

This should seem all the more puzzling in light of Schnitzer's result[4,21] that

* Recall that the S-wave T-matrix is related to the scattering length a near threshold via $\mathbf{T} = \frac{1}{2i}(\exp(2iak) - \mathbf{1})$, where k is the pion momentum.

chiral soliton models must necessarily obey all soft-pion theorems, of which Weinberg's is a notable example.

Actually, there is no contradiction. To see this, recall that the equality of the amplitudes implied by (20*b*) is only valid to order N^0. But the right-hand side of Eq. (24) is manifestly of order $1/N$. Thus Eqs. (24) and (25) are both trivially satisfied to order N^0: to this order, $a_{I=\frac{1}{2}} = a_{I=\frac{3}{2}} = 0$! A nontrivial consistency check of Weinberg's theorem, then, must await a higher-order calculation.

Confronting Experiment: $\pi N \to \pi\Delta$

We turn next to an examination of $\pi N \to \pi\Delta$, drawing from the recent partial-wave analysis of Manley *et al.*[22] The data presented there are restricted to $W \leq 2$ GeV and $L \leq 3$.

We begin by looking at processes in which the pion jumps two units of angular momentum. From Eq. (22) we predict simple proportionality relations between partial-wave amplitudes:†

$$SD_{11} = -\sqrt{2} \cdot DS_{13} = -\sqrt{10} \cdot SD_{31} = \sqrt{20} \cdot DS_{33} \tag{26a}$$

and

$$FP_{15} = -\sqrt{10} \cdot FP_{35}. \tag{26b}$$

These relations are checked in Fig. 5. For the SD and DS waves, the agreement is not impressive. The relative signs of the four amplitudes are predicted correctly, but there is no evidence for the factor of $\sqrt{10}$ which connects the first and second pairs of terms in Eq. (26a). One should note that these channels all couple to the translation zero-modes. For the FP waves, which do not, the agreement is quite satisfactory, modulo the customary 150-200 MeV energy shift between the isospin-$\frac{1}{2}$ and the isospin-$\frac{3}{2}$ amplitudes.

We turn next to processes for which the initial and final pion angular momenta are equal. In both the D- and F-waves, the partial-wave amplitudes for only three out of the four possible channels could be resolved from the data in the analysis of Ref. 22. These triplets of amplitudes are predicted to obey

† The notation is $LL'_{2I,2J}$, with L and L' the incoming and outgoing pion angular momenta, respectively. Unfortunately, Ref. 22 does not present amplitudes for the two PF channels.

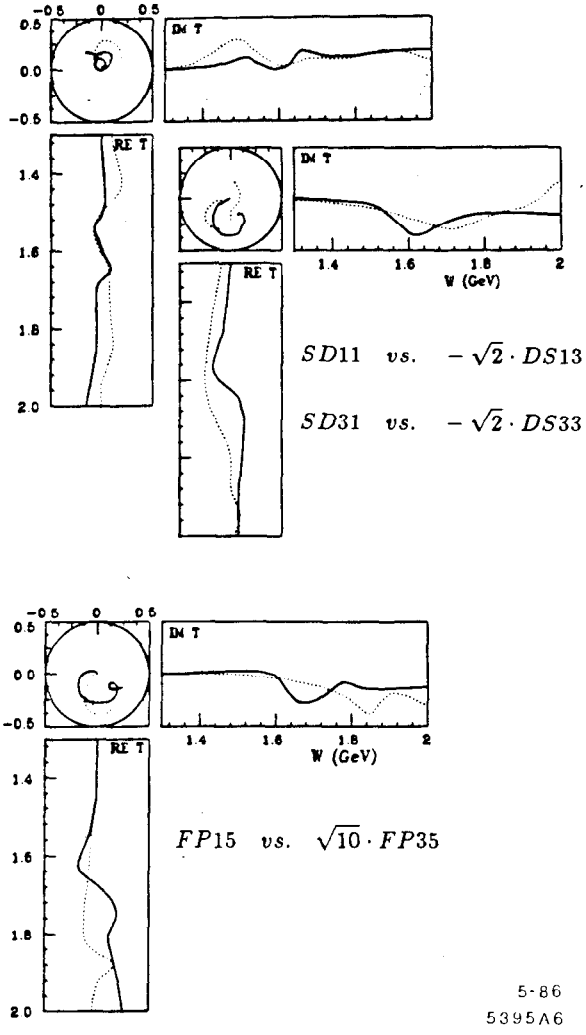

Fig. 5 (from Ref. 8). $\pi N \to \pi\Delta$ processes in which the pion jumps two units of angular momentum: (a) Test of Eq. (26a) by comparison of the various SD and DS $\pi N \to \pi\Delta$ partial-wave amplitudes. The upper graph plots SD_{11} against $-\sqrt{2}\cdot DS_{13}$; the lower graph plots SD_{31} against $-\sqrt{2}\cdot DS_{33}$. (b) Test of Eq. (26b) by comparison of FP_{15} to $-\sqrt{10}\cdot FP_{35}$. In each case, the first-named amplitude is represented by the solid curve.

the relations:

$$DD_{33} = \frac{4}{5\sqrt{10}}\cdot DD_{13} + \frac{9}{10}\sqrt{\frac{7}{5}}\cdot DD_{15} \qquad (27a)$$

and

$$FF_{37} = \frac{7}{6\sqrt{6}} \cdot FF_{15} + \frac{2}{3}\sqrt{\frac{5}{3}} \cdot FF_{35}. \qquad (27b)$$

In Fig. 6 we have displayed the experimental DD_{33} and FF_{37} amplitudes (indicated by solid lines) juxtaposed with the appropriate linear combinations dictated by (27) (dotted lines). Although in the first instance (where again there is mixing with the translational mode) the shape of the Argand plot is reasonably rendered, the predicted curve is obviously too big by roughly a factor of four. In the second case, however, as for F-waves in general, the agreement is quite respectable.

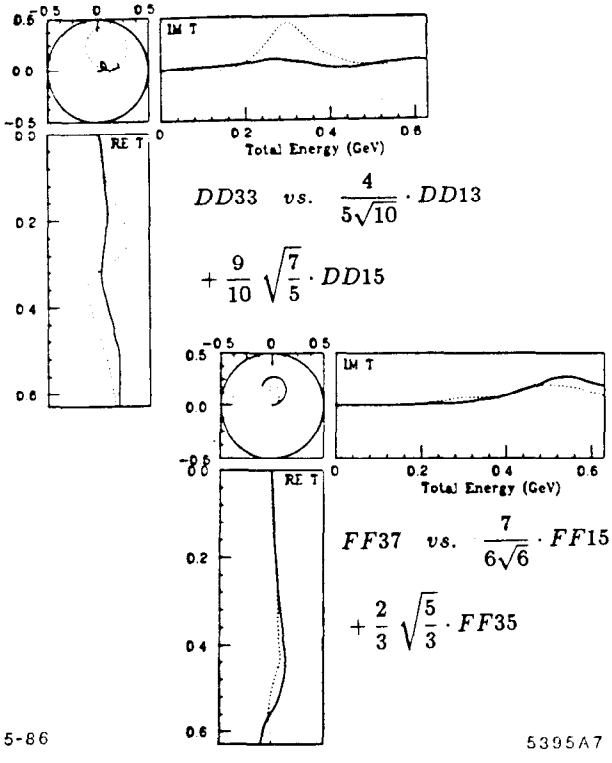

Fig. 6 (from Ref. 8). $\pi N \to \pi\Delta$ processes in which the initial and final pion angular momenta are equal. The DD_{33} and FF_{37} amplitudes (solid lines) are juxtaposed with the linear combinations to which they are predicted to correspond via Eq. (27) (dotted lines).

Unfortunately, out of the four possible PP processes, only PP_{11} and PP_{33} were considered by Manley, *et al.*, to be adequately determined by the data. This makes it impossible for us to test the validity of Eq. (21) for this case. If, however, we assume the PP_{13} amplitude to be small, Eq. (21b) suggests that

the PP_{11} and PP_{33} amplitudes will have the same sign; this is indeed what is observed experimentally. We turn, finally, to Eq. (23), which links the processes $\pi N \to \pi N$ and $\pi N \to \pi\Delta$. The relations can be expressed as:

$$\frac{1}{\sqrt{2}}(P_{11} - P_{13}) = \frac{5}{4} \cdot PP_{33} - \frac{1}{8} \cdot PP_{11}; \tag{28a}$$

$$\frac{1}{\sqrt{2}}(D_{13} - D_{33}) = \frac{9}{10\sqrt{2}} \cdot DD_{13} + \frac{9\sqrt{7}}{20} \cdot DD_{15}; \tag{28b}$$

$$\frac{1}{\sqrt{2}}(F_{15} - F_{17}) = \frac{1}{2} \cdot FF_{35} + \sqrt{\frac{3}{5}} \cdot FF_{37}. \tag{28c}$$

The left- and right-hand sides of these equations, corresponding to $\pi N \to \pi N$ and $\pi N \to \pi\Delta$, are compared in Fig. 7; they are indicated by solid and dotted lines, respectively. Once again, although the sizes of the amplitudes are not in especially close agreement, the signs are correctly given and the general shapes are similar.

All in all, we can conclude that the limited $\pi N \to \pi\Delta$ data, while not as compelling as $\pi N \to \pi N$, is certainly consistent with the elegant interpretation of the baryon as a soliton in the field of pions.

5. The Baryon Spectrum of the Skyrme Model

In this Section we shall apply the formalism developed in Section 3 to the particular case of the Skyrme Lagrangian:[1]

$$\mathcal{L} = \frac{f_\pi^2}{16} \operatorname{Tr} \partial_\mu U \partial_\nu U^\dagger + \frac{1}{32e^2} \operatorname{Tr}[(\partial_\mu U)U^\dagger, (\partial_\nu U)U^\dagger]^2. \tag{29}$$

Here f_π is the pion decay constant (186 MeV in the real world) and e is a new, dimensionless coupling constant peculiar to the model; our approach will be to treat both as adjustable parameters, in order to see how close we can get to reproducing the observed baryon mass spectrum. The "small parameter" $1/N$ enters the Lagrangian through f_π and e, which behave like $N^{\frac{1}{2}}$ and $N^{-\frac{1}{2}}$ in the large-N limit, respectively.

To study this model, one need not be motivated by the belief that it is in any way "fundamental" (*i.e.*, derivable from QCD). Rather, it is instructive to see how well the actual spectrum of nucleon and Δ resonances can be fit starting from a simple, tractable model that contains no explicit quark or baryon fields and only two adjustable parameters. Pleasingly, the spectrum that emerges

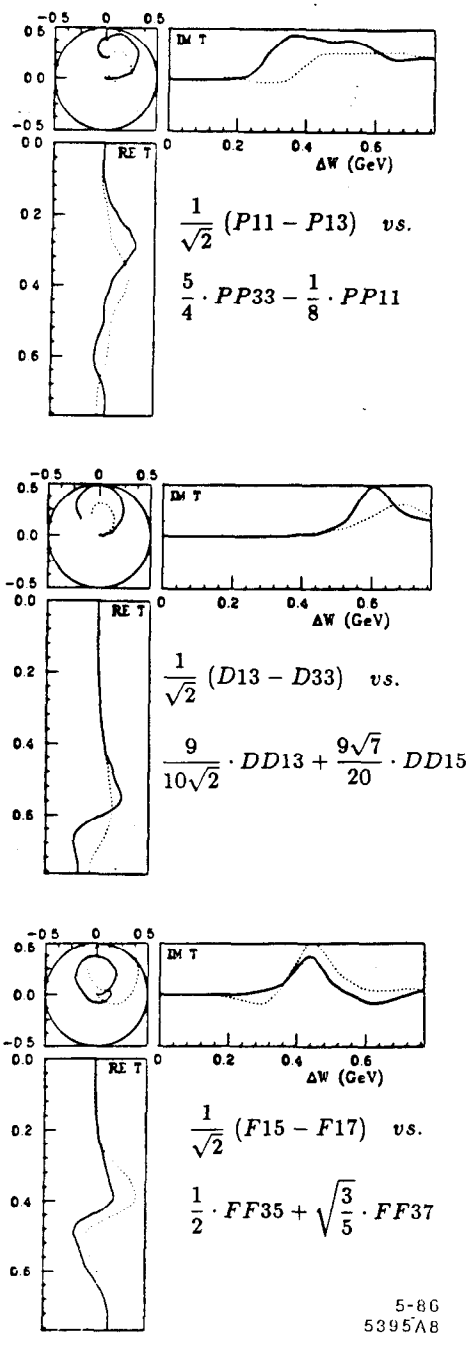

Fig. 7 (from Ref. 8). Comparison of $\pi N \to \pi N$ and $\pi N \to \pi \Delta$ scattering in the same partial wave. The linear combinations of elastic amplitudes (solid lines) are juxtaposed with the appropriate combinations of inelastic amplitudes (dotted lines) as dictated by Eq. (28).

is, on the whole, in good agreement with the real world for energies up to 3 GeV. This is all the more surprising given the rather drastic nature of our approximations, such as completely neglecting baryon recoil (*cf.* Section 2).

As always, we shall focus on the hedgehog solution

$$U_0 = e^{iF(r)\hat{\mathbf{r}}\cdot\vec{\sigma}}, \tag{30}$$

where $F(r)$ solves a (hopefully familiar) variational equation. If we plug this ansatz into (29) and look at small fluctuations about the soliton

$$F(r)\hat{\mathbf{r}} \longrightarrow F(r)\hat{\mathbf{r}} + \frac{2}{f_\pi}\vec{\pi}(\mathbf{x},t) \tag{31}$$

we obtain an expression such as Eq. (7), with $\widehat{\mathbf{L}}$ a complicated 3×3 matrix of second-order linear differential operators.

As discussed in Section 3, we can make substantial progress by expanding the pion field in eigenstates of $\mathbf{K}^2$ and K_z. Explicitly, this is accomplished by plugging

$$\vec{\pi}(\mathbf{x},t) = \sum_{K,K_z} \Big\{ \psi_-^{KK_z}(r,t)\mathbf{\Pi}_{K-1}^{KK_z}(\Omega) + \psi_0^{KK_z}(r,t)\mathbf{\Pi}_K^{KK_z}(\Omega) + \psi_+^{KK_z}(r,t)\mathbf{\Pi}_{K+1}^{KK_z}(\Omega) \Big\} \tag{32}$$

into (7); here $\mathbf{\Pi}_L^{KK_z}$ are the so-called "vector spherical harmonics," defined by:

$$\mathbf{\Pi}_L^{KK_z} = \begin{pmatrix} \langle L1K_z-1,1|K,K_z\rangle\, Y_{L,K_z-1}(\Omega) \\ \langle L1K_z0|K,K_z\rangle\, Y_{L,K_z}(\Omega) \\ \langle L1K_z+1,-1|K,K_z\rangle\, Y_{L,K_z+1}(\Omega) \end{pmatrix}. \tag{33}$$

Parity precludes the ψ_0's from mixing with the $\psi_\pm$'s; ψ_+ and ψ_- can mix in this model, however, as they do in Nature, where jumps of two units of pion angular momentum are allowed in the process $\pi N \to \pi\Delta$.

It turns out that the integration over solid angles in Eq. (7) can be performed in closed form, thanks to some standard identities for differentiating

spherical harmonics. We are left with an expression for the action of the form

$$S = -\int dt\, m_0 + \sum_{K,K_z} \int r^2 dr \psi_0^{KK_z*}(r,t) \hat{L}_0^K \psi_0^{KK_z}(r,t)$$

$$+ \sum_{K,K_z} \int r^2 dr \left(\psi_-^{KK_z*}(r,t), \psi_+^{KK_z*}(r,t)\right) \begin{pmatrix} \hat{L}_{--}^K & \hat{L}_{-+}^K \\ \hat{L}_{+-}^K & \hat{L}_{++}^K \end{pmatrix} \begin{pmatrix} \psi_-^{KK_z}(r,t) \\ \psi_+^{KK_z}(r,t) \end{pmatrix}. \tag{34}$$

Note that the $\hat{L}^K$'s, complicated though they be, are now second-order linear differential operators in r and t alone. We will refer to the 2×2 matrix of operators here as $\hat{\mathbf{L}}^K$ and the 2-component column-vector of wavefunctions as Ψ^K.

The determination of the reduced amplitudes $\mathcal{T}_{KL'L}$ now proceeds in a completely straightforward manner, exactly as in ordinary potential scattering. The "normal-mode" equations to be solved are

$$\hat{L}_0^K \left[\psi_0^K(r) e^{i\omega t}\right] = 0 \tag{35a}$$

and

$$\hat{\mathbf{L}}^K \left[\Psi^K(r) e^{i\omega t}\right] = 0 \tag{35b}$$

for all ω; here we are assuming that $\hat{L}$ and $\hat{\mathbf{L}}$ have been chosen with care to be self-adjoint.

Let us consider Eq. (35a) first. It suffices to consider the radial wavefunctions that are well behaved at the origin and to integrate out past the point where the skyrmion profile $F(r)$ is negligible. In this regime the theory is one of free pions, so ψ_0^K can be fit to* $A(\omega) j_K(\omega r) + B(\omega) n_K(\omega r)$. $\mathcal{T}_{KKK}$ can then be extracted by rewriting this as

$$\text{constant} \times \left[h_K^- - (2i\mathcal{T}_{KKK}(\omega) + 1) h_K^+\right] \tag{36}$$

yielding

$$\mathcal{T}_{KKK}(\omega) = -\frac{1}{2i}\left[(B + iA)^{-1}(B - iA) + 1\right]. \tag{37}$$

The '2×2' case (35b) proceeds analogously. Near the origin for each $K \geq 1$ there are two independent regular solutions Ψ_1^K and Ψ_2^K, which behave

* We follow Messiah[23] in our definitions of the spherical Bessel functions.

asymptotically as

$$\tilde{\Psi}_i^K \sim \begin{pmatrix} A_i(\omega) j_{K-1}(\omega r) + B_i(\omega) n_{K-1}(\omega r) \\ -C_i(\omega) j_{K+1}(\omega r) - D_i(\omega) n_{K+1}(\omega r) \end{pmatrix} \qquad i = 1, 2. \tag{38}$$

If we work in the convenient basis in which the incoming pions are in pure $(K-1)$-waves or $(K+1)$-waves of orbital angular momentum, we find:

$$\begin{pmatrix} \mathcal{T}_{K,K-1,K-1} & \mathcal{T}_{K,K-1,K+1} \\ \mathcal{T}_{K,K+1,K-1} & \mathcal{T}_{K,K+1,K+1} \end{pmatrix}$$

$$= -\frac{1}{2i}\left[\begin{pmatrix} B_1 + iA_1 & D_1 + iC_1 \\ B_2 + iA_2 & D_2 + iC_2 \end{pmatrix}^{-1} \begin{pmatrix} B_1 - iA_1 & D_1 - iC_1 \\ B_2 - iA_2 & D_2 - iC_2 \end{pmatrix} + \mathbf{1} \right]. \tag{39}$$

The details of this procedure, including explicit expressions for the unwieldy differential operators involved, can be found in Refs. 7 and 14. As an illustration of the numerical results, Fig. 8 depicts the five reduced amplitudes that contribute to physical G-wave scattering. Note that $\mathcal{T}_{544}$ is almost completely negligible compared with $\mathcal{T}_{344}$ and $\mathcal{T}_{444}$; we will make crucial use of this observation in Section 6.

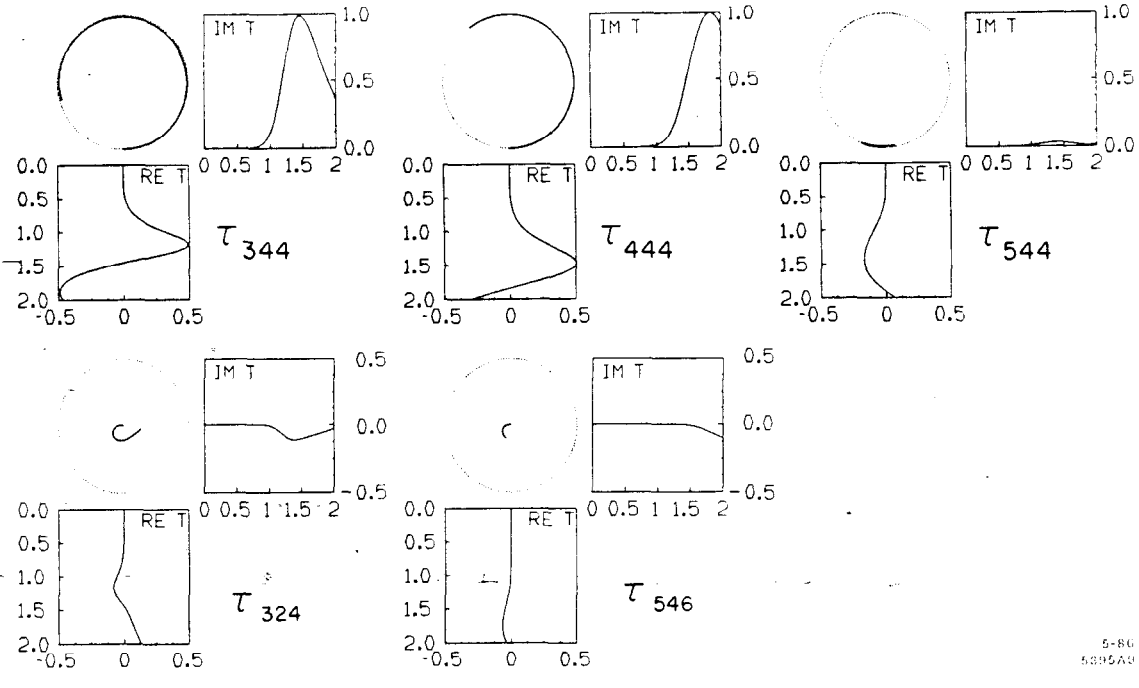

Fig. 8 (from Ref. 13). The five reduced amplitudes that couple to the G waves.

Confronting Experiment: $\pi N \to \pi N$

So far we have discussed the (linearized) equations of motion for pions moving in a fixed external skyrmion background. To relate this to physical πN scattering requires the use of Eqs. (18)-(19). The resulting Argand plots for $\pi N \to \pi N$ are presented in Fig. 9, together with the corresponding experimental results as drawn from Refs. 20 and 24. For future reference, Fig. 9 also presents the amplitudes that emerge from the 3-flavor Skyrme model, which is taken up in Sections 8-9.

The overall degree of agreement with experiment evident in Fig. 9 is remarkable. The F waves are especially well reproduced by the model—these are the first channels that do not mix with the skyrmion's zero-modes. Much of the disagreement in the higher waves can obviously be accounted for by the fact that our simplistic formalism does not allow for the wide variety of inelastic processes that occur in the real world; consequently our Argand plots stick too closely to the rim of the unitarity circle, and are simply much too large. Ideally one should allow for multiple pion production, other mesons and/or strangeness.

Particularly striking is the pattern of size alternation displayed by the experimental amplitudes and by their Skyrme-model counterparts for each value of L. For example, in the F waves, the F_{15} and F_{37} amplitudes move much more vigorously through the unitarity circle than do the F_{17} and F_{35}. We shall return to this "big-small-small-big" pattern in Section 6, where we shall see that it finds a natural explanation in the framework of skyrmion physics.

We should, however, squarely confront the Skyrme model's failures; these lie in the S- and P-waves. Indeed one's natural inclination is to turn first to the P_{33} channel, where in one of the cleanest examples of elastic scattering in Nature the Δ manifests itself dramatically as a full rotation around the unitarity circle. Instead, one finds in the Skyrme model initial *repulsive* (*i.e.*, clockwise) behavior. A similar sad story is to be found in the P_{11} channel; this is where the second-lightest resonance, the "Roper" at 1440 MeV, appears in Nature. Interestingly, the poor performance of the Skyrme model in the P-wave sector was first noticed by Skyrme himself:

> The P-wave meson-particle interaction [is] repulsive on the average. There is no indication of the strong attraction observed in the pion-nucleon resonant state, but this would hardly be expected in a static classical treatment where the rotational splitting of the particle states has been ignored.[2]

Yet these failures are not necessarily fatal for the model. For, despite the large discrepancies, one can argue that $1/N$ perturbations in the P-wave sector

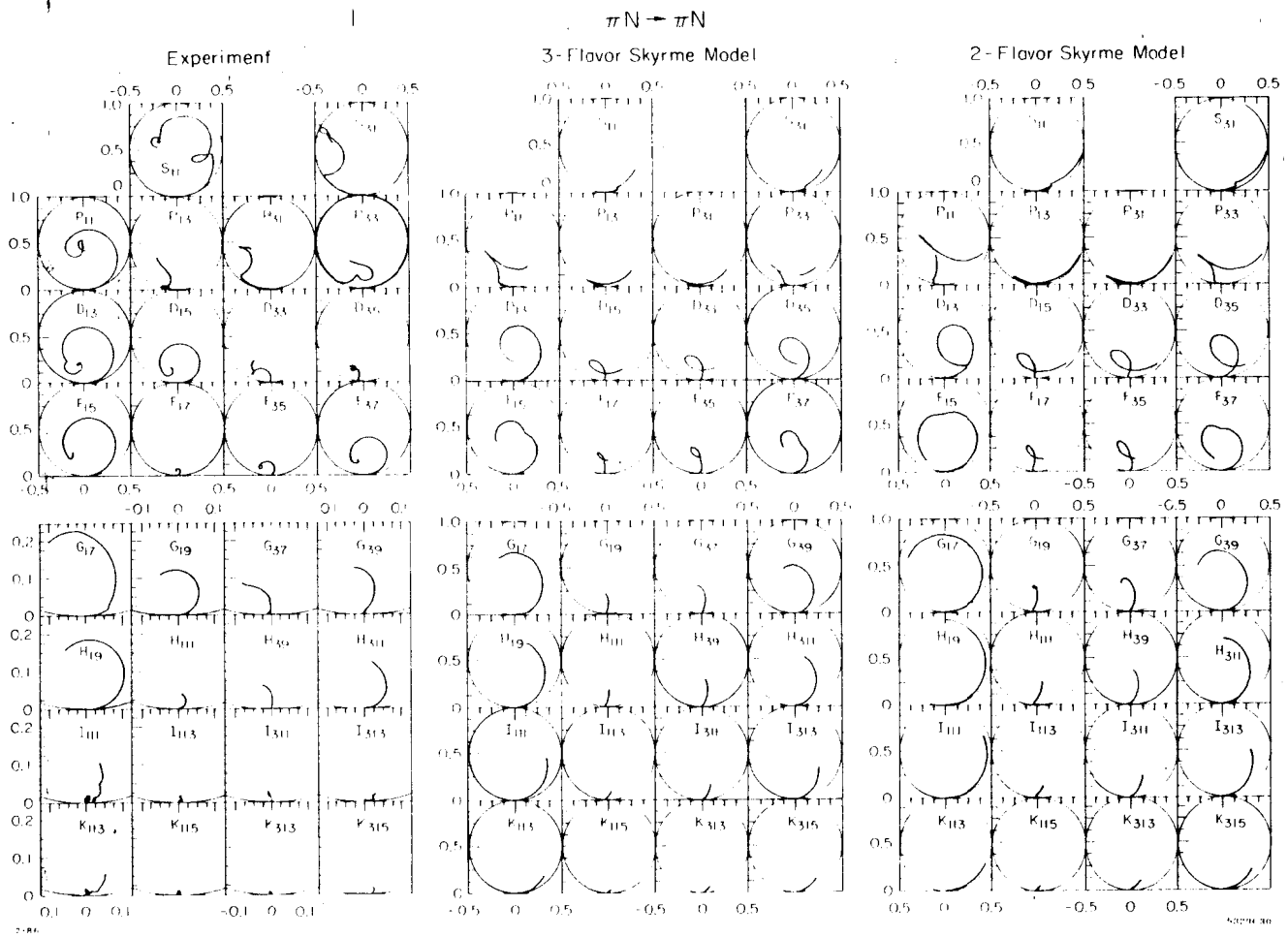

Fig. 9 (from Ref. 13). $\pi N \to \pi N$: comparison between the 2- and the 3-flavor Skyrme models and the experimental solutions of: (*i*) Ref. 24 for $L \leq 5$; (*ii*) Ref. 20 for $6 \leq L \leq 7$. The plots show Im(T) *vs.* Re(T) for each channel. Channels are labeled by $L_{2I,2J}$, where L is the pion angular momentum, I is the total isospin and J the total angular momentum. Note the change of scale for the experimental graphs with $L \geq 4$.

of the theory can cause enormous effects in the corresponding Argand plots which could easily produce the observed real-world behavior for the amplitudes.

To see this, note that the physical P-wave amplitudes (P_{11} and P_{33} especially) all contain contributions from the reduced amplitude T_{111}, as is apparent from (19). This is the channel to which the rotational zero-modes of the skyrmion couple at threshold (see Section 3). As a result, in the model, the S-matrix has a pole and a zero that have coalesced at the origin of the energy-plane for all four P-wave channels of πN scattering. Now, one can easily envision effects which perturb these poles and zeroes away from the origin; certainly the quantization of the collective coordinates, which involves the next order in the $1/N$ expansion, is one such effect. Consequently some of these poles might end up in the fourth quadrant, slightly below the positive real axis (Fig. 10*a*), while others might be pushed into the second quadrant (Fig. 10*b*). (These are quadrants of the 'second sheet.')

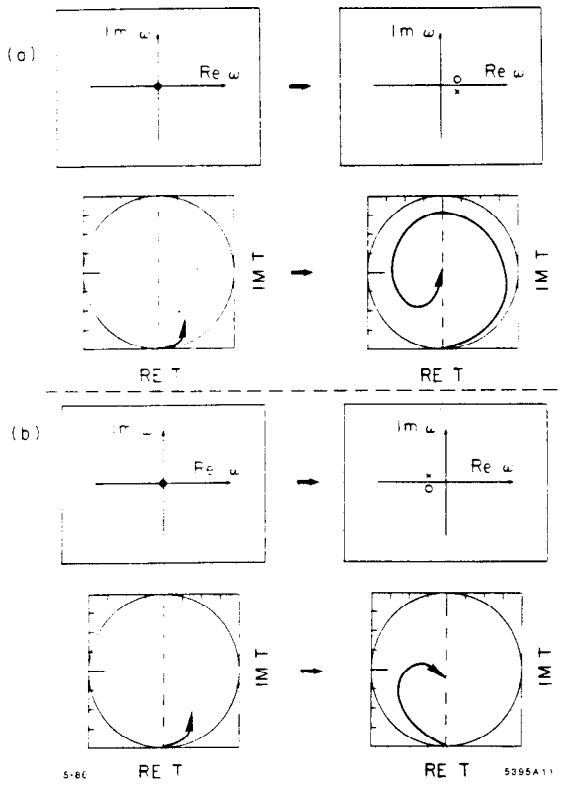

Fig. 10 (from Ref. 7). Possible movement due to $1/N$ corrections of the poles and zeroes of the S-matrix in the complex energy-plane, and the resulting effects on the amplitude near threshold. Poles are denoted by a cross and zeroes by a circle.

If this scenario actually takes place in the real world, what would we actually observe? The channels in which the poles have been perturbed into the fourth quadrant would contain clear P-wave resonances lying reasonably close to threshold: suggestively, the resonances our model lacks to lowest order, namely the $\Delta(1232)$ and the $N(1440)$, are in fact the two lowest-lying excitations in πN scattering. In contrast, the channels in which the poles have been pushed into the second quadrant would be characterized by precisely the kind of *repulsive* behavior at low energies that one finds in the P_{13} and P_{31} amplitudes. Thus our scenario gives at least a consistent interpretation of the real-world P-wave amplitudes near threshold.

In a sense we already know that the Δ pole *must* be pushed into the fourth quadrant by such higher-order corrections. This is evident in Eq. (4), according to which the nucleon-Δ mass-difference is proportional to $e^3 f_\pi$ and hence of order $1/N$. In contrast, the typical excitation energies obtained in the leading-order phase-shift analysis of this Section are measured in units of ef_π which is of order N^0. Thus it would actually have been *inconsistent* for the Δ to have appeared as a resonance above threshold in our lowest-order calculation, since, to this order, the nucleon and Δ are degenerate.

Before leaving the P-waves, we ought to point out that the P_{13} and P_{31} amplitudes are already given quite nicely. Indeed, the standard lore is that the repulsive regions of Argand diagrams are very difficult to concoct in quark models of resonances, and so we consider it especially satisfactory to find such behavior emerging automatically from such a simple model.

We turn next to the S-wave channels, where the model fails to reproduce the observed initial repulsive behavior of the amplitude in the S_{31} channel. But the S-waves couple to the *translational* modes of the soliton, as discussed in Section 3. Thus just as for the P-waves one can argue that a small perturbation of the form depicted in Fig. 10*b* could readily induce the desired behavior. Indeed, we saw explicitly in Section 4 that the repulsive threshold behavior of the S_{31} amplitude is a $1/N$ effect (*cf.* Eq. (24)).

In sum, although we initially set out to explain the severe discrepancies between the Skyrme model and experiment in the lower partial waves, we have actually accomplished much more: we have outlined a framework according to which the real-world behavior of the S- and P-wave amplitudes near threshold can be understood as arising from higher-order corrections in an underlying chiral-soliton model such as Skyrme's. In particular, repulsive behavior near threshold arises in this picture from S-matrix poles that have been perturbed from the origin into the first or second quadrant, while strong low-lying resonances arise from poles perturbed into the fourth quadrant.

Returning to the Skyrme model, we can, of course, extract resonance

masses in a straightforward manner from the partial-wave phase-shifts. These masses will be functions of the adjustable parameters e and f_π, which can then be optimized *vis-à-vis* experiment according to several different prescriptions. Our preferred approach has been to perform a least-squares fit to the experimental masses, with all resonances, including the nucleon and Δ, weighted equally. The resulting mass spectrum is presented in Fig. 11. The optimal values for the Skyrme parameters calculated in this manner turn out to be $\{e = 4.79, f_\pi = 150$ MeV$\}$. An alternative prescription adopted by Adkins, Nappi and Witten[3] is to choose e and f_π in such a way as to fix just the proton and the Δ masses to their experimental values, but this yields a much poorer fit to the spectrum as a whole. (This is not too surprising since specifying the nucleon-Δ mass-difference involves a fine-tuning to order $1/N$.) Pleasingly, the values given above for e and f_π greatly improve many of the *static* properties of the model as well compared with Adkins, Nappi and Witten,* at the expense of allowing a proton mass of 1190 MeV. In light of our earlier discussion, we have chosen in Fig. 11 to compare our lowest-lying $\mathcal{O}(N^0)$ excitations in the P_{11} and P_{33} channels, *not* with the Roper and the Δ, which are only split from the nucleon in $\mathcal{O}(1/N)$, but rather with the next-higher resonances in those channels, which lie at 1700 and 1600 MeV, respectively;† our "prediction" in Fig. 11 for m_Δ (as for m_N) merely come from Eq. (4).

It is interesting that, even in those channels where the amplitudes are not reproduced very well, the model accurately predicts the resonance masses. In fact, most of the masses are given to within 6% of their quoted values. This holds all the way up to 3 GeV, which is surprising for a "low-energy" theory.

Confronting Experiment: $\pi N \to \pi\Delta$

We can also use Eq. (18) to obtain Skyrme-model amplitudes for the process $\pi N \to \pi\Delta$. Figure 12 displays the experimental $\pi N \to \pi\Delta$ curves, drawn from Ref. 22, compared with both the 2- and 3-flavor Skyrme-model predictions. As in the elastic case, the agreement is surprisingly good. In fact, there is 100% accord in the signs of the $\pi N \to \pi\Delta$ amplitudes—a significant improvement over $SU(6)$.[22] The correctly-rendered minus-sign in the DD_{13} channel is especially gratifying, in view of the fact that all other PP, DD and FF graphs lie in the upper-half plane. It is also noteworthy that, in both the model and experiment, the FF_{15} amplitudes circle around much more than the FF_{35} and FF_{37} curves.

---

* See Table II of Ref. 7.

† Interestingly, the most recent partial-wave analysis[25] finds no evidence for the $N(1700)$, but instead finds a state at roughly 1500 MeV—in much closer agreement with the Skyrme-model prediction.

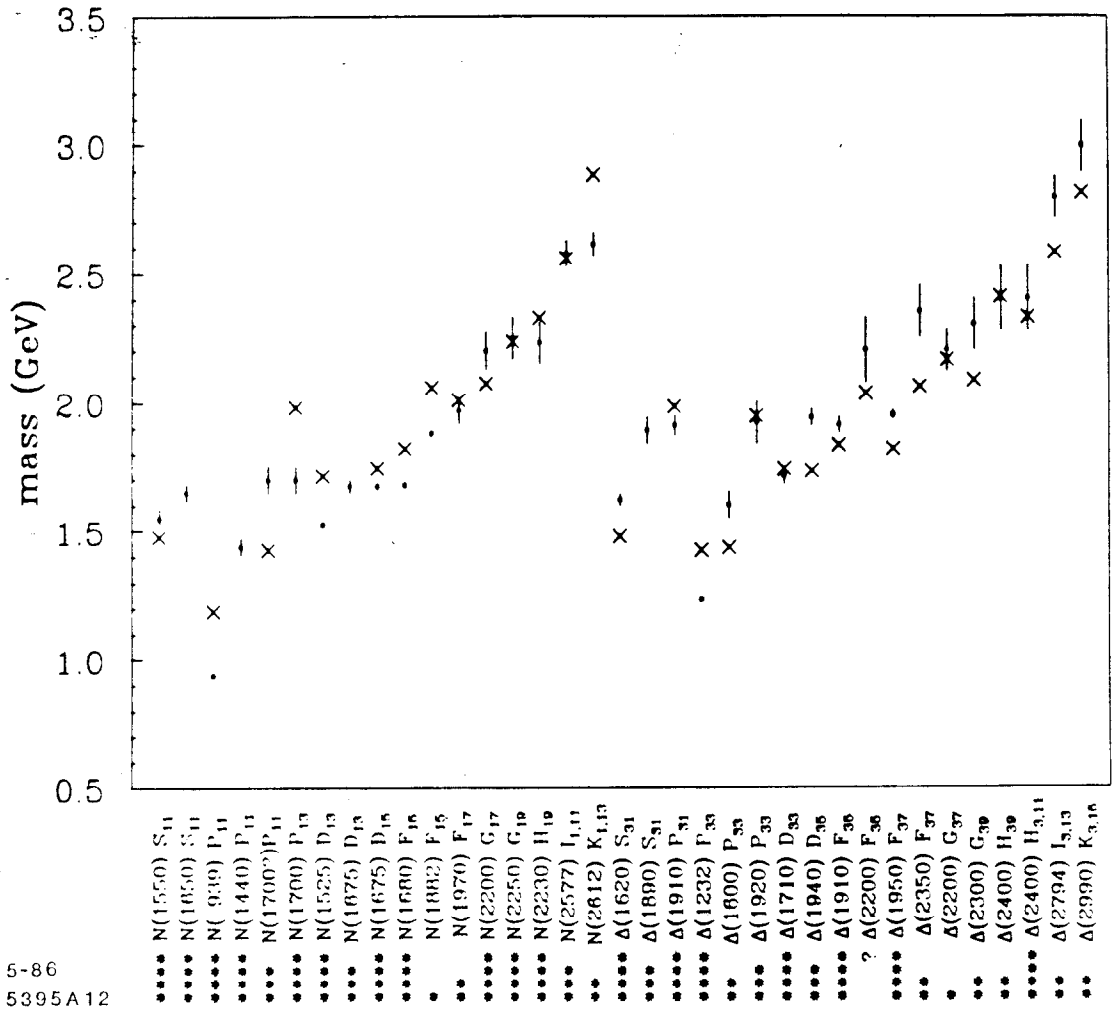

Fig. 11 (from Ref. 13). Spectrum of N and Δ resonances: Skyrme model *vs.* experiment. The experimental masses (indicated by dots) and uncertainties are taken from Ref. 24, except for the $N(1882)$ F_{15} and the four I- and K-wave states, which are taken from Ref. 20. The Skyrme-model predictions of Refs. 7 and 12 are indicated by crosses. In general, the 2- and 3-flavor predictions are identical; the exceptions are the $N(1882)$ F_{15} and the $\Delta(2350)$ F_{37}, which only exist in the 3-flavor Skyrme model.[12] Resonances have been assigned stars in accord with the Particle Data Group, ranging from four stars for the best established down to one star for the least well established states. The most recent analysis[25] finds no evidence for the $N(1700)$ P_{11}, but instead finds a state near 1500 MeV. Also shown are the four observed 3- or 4-star resonances which have no Skyrme-model counterparts in our analysis, namely the $N(1650)$ S_{11}, the $N(1440)$ P_{11}, the $N(1675)$ D_{13}, and the $\Delta(1890)$ S_{31}. The Skyrme-model values for m_N and m_Δ are obtained from Eq. (9) of Ref. 3, using our "best fit" parameters $\{e = 4.79,\ f_\pi = 150\,\mathrm{MeV}\}$.

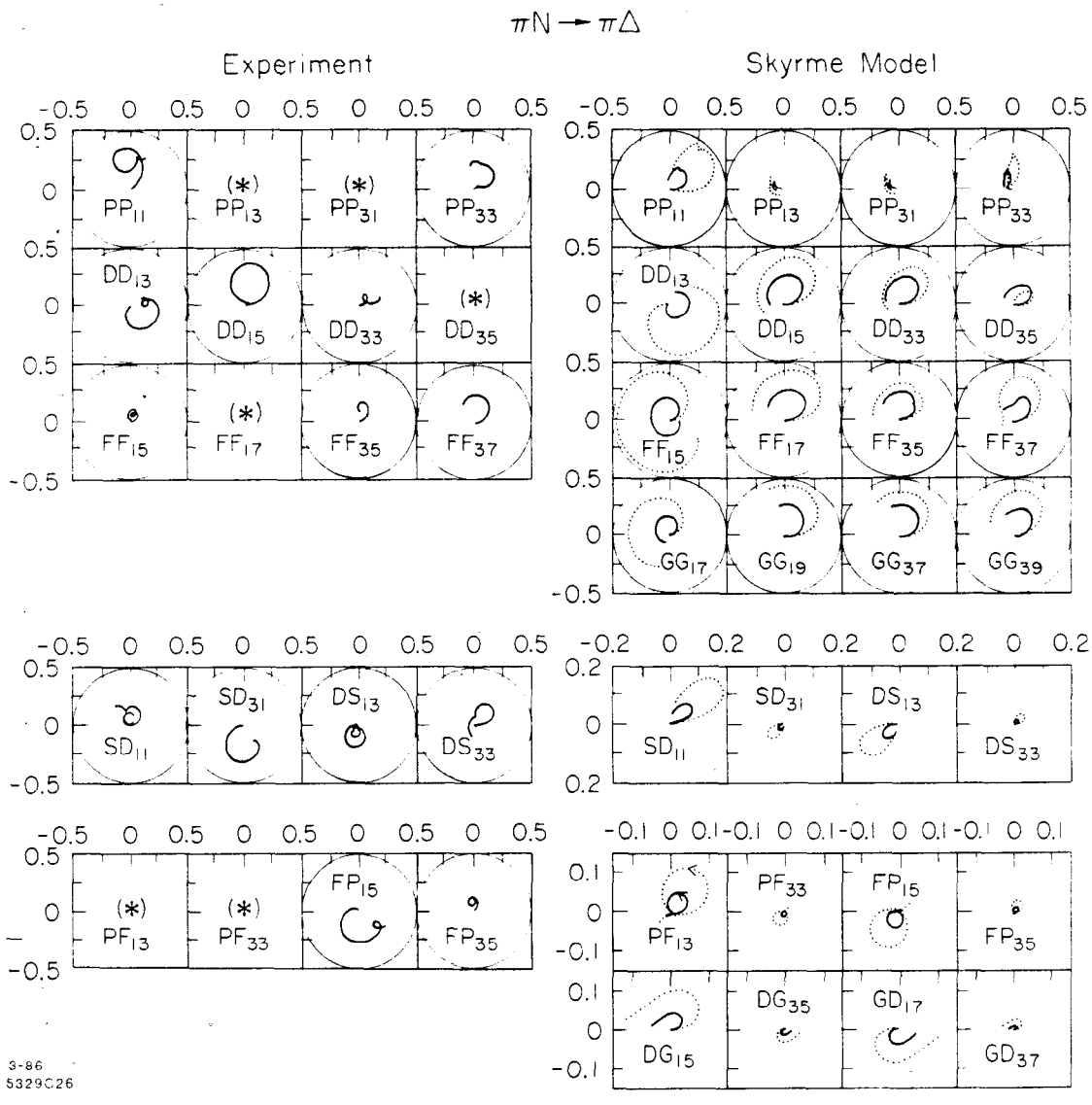

Fig. 12 (from Ref. 13). $\pi N \to \pi\Delta$: comparison between the 2- and the 3-flavor Skyrme models and the experimental solution of Ref. 22. Channels are labeled by $LL'_{2I,2J}$, with L and L' the incoming and outgoing pion angular momenta, respectively. 3-flavor Skyrme model results are depicted by solid lines, 2-flavor results by dotted lines. An asterisk denotes amplitudes which were found to be small and/or poorly determined by the available data, and were therefore not included in the experimental solution. Note change of scale for Skyrme-model plots with $L' = L \pm 2$.

6. The Big-Small-Small-Big Pattern

In this Section, we examine more closely the big-small-small-big pattern displayed by the elastic πN partial-wave amplitudes in both the Skyrme model and experiment. Specifically, for each value of L, the excursion of the amplitude into the unitarity circle is nearly always much larger for the $(I,J) = (\frac{1}{2}, L-\frac{1}{2})$ or $(\frac{3}{2}, L+\frac{1}{2})$ channels than for $(\frac{1}{2}, L+\frac{1}{2})$ or $(\frac{3}{2}, L-\frac{1}{2})$. (The glaring exception is the D_{35} curve.)

Clearly, this pattern of size alternation is consistent with the model independent Eqs. (20*a*) and (20*b*), since, in these equations, the $(\frac{3}{2}, L-\frac{1}{2})$ and $(\frac{3}{2}, L+\frac{1}{2})$ amplitudes are linked by large coefficients to the $(\frac{1}{2}, L+\frac{1}{2})$ and $(\frac{1}{2}, L-\frac{1}{2})$ amplitudes, respectively. But of course, the reversed pattern, with the two "small" and two "big" channels interchanged, would have been equally consistent. For a more compelling argument, one must necessarily go beyond the purely group-theoretic reasoning that led to (20) and add a single plausible *dynamical* assumption.

To this end, let us return to Eq. (19), in which the physical $\pi N \to \pi N$ amplitudes for each L are expressed as linear combinations of the reduced amplitudes $\mathcal{T}_{KLL}$ with $K = L-1, L, L+1$. Now, in the specific case of the Skyrme model, it turns out that $\mathcal{T}_{L+1,LL}$ is essentially negligible compared to $\mathcal{T}_{L-1,LL}$ and $\mathcal{T}_{LLL}$, as was illustrated in Fig. 8 for the case of the G-waves. Certainly it is plausible to assume that this continues to be true for the (unknown) optimal two-flavor effective Lagrangian of Nature, $\mathcal{L}_{\rm opt}$. Accordingly, let us make the dynamical assumption that

$$\mathcal{T}_{L+1,LL} \approx 0 \tag{40}$$

in Eq. (19). The pattern of alternating size then emerges as an automatic consequence of the group theory: it is simply due to the relatively small coefficients multiplying $\mathcal{T}_{L-1,LL}$ and $\mathcal{T}_{LLL}$ in (19b) and (19c) compared to (19a) and (19d)! A further prediction of these expressions is that, of the two "big" amplitudes, $\mathbf{T}^{\pi N \pi N}_{L\frac{1}{2},L-\frac{1}{2}}$ should dominate $\mathbf{T}^{\pi N \pi N}_{L\frac{3}{2},L+\frac{1}{2}}$ since the coefficients in the first case are a little bigger—and, with the single exception of the problematic P-waves, this is also apparent in Fig. 9.

In short, the big-small-small-big pattern finds a natural explanation in the chiral-soliton framework, *viz.*, that the reduced amplitude $\mathcal{T}_{L+1,LL}$ is negligible compared to $\mathcal{T}_{L-1,LL}$ and $\mathcal{T}_{LLL}$, both for the Skyrme model and for $\mathcal{L}_{\rm opt}$.

Fortunately, we have the means of testing whether this dynamical assumption is a valid approximation for $\mathcal{L}_{\rm opt}$. For, with $\mathcal{T}_{L+1,LL}$ set to zero, Eq. (18) can be shown to imply an *additional* model-independent linear relation between

$\pi N \to \pi N$ and $\pi N \to \pi\Delta$:

$$3L\mathbf{T}^{\pi N\pi N}_{L\frac{1}{2},L-\frac{1}{2}} + (L+2)\mathbf{T}^{\pi N\pi N}_{L\frac{1}{2},L+\frac{1}{2}}$$
$$\cong 3L\sqrt{\frac{2L-1}{L+1}}\mathbf{T}^{\pi N\pi\Delta}_{LL\frac{1}{2},L-\frac{1}{2}} + (10L+11)\sqrt{\frac{L}{2L+3}}\mathbf{T}^{\pi N\pi\Delta}_{LL\frac{1}{2},L+\frac{1}{2}}. \qquad (41)$$

Figure 13 tests this relation as applied to the experimental $\pi N \to \pi N$ [20] and $\pi N \to \pi\Delta$ [22] P-, D- and F-wave amplitudes. It should be noted that the agreement in the *signs* of the amplitudes evident in Fig. 13 is in itself a nontrivial result. For the P and F waves, the relation appears rather well satisfied. In particular, it works roughly as well as Eq. (23) (see Fig. 7), which likewise relates $\pi N \to \pi N$ and $\pi N \to \pi\Delta$, but was derived *without* the additional dynamical approximations (40). Unlike Eq. (23), however, there is poor agreement evident in Fig. 13 in the D waves—which is *consistent* with the fact that the big-small-small-big pattern itself does not work well for the D waves (*cf.* Fig. 9.)

Our conclusion, suggested by the big-small-small-big pattern and reinforced by Fig. 13, is that the dynamical assumption (40) is (with the probable exception of the D waves) a valid approximation for $\mathcal{L}_{\rm opt}$.

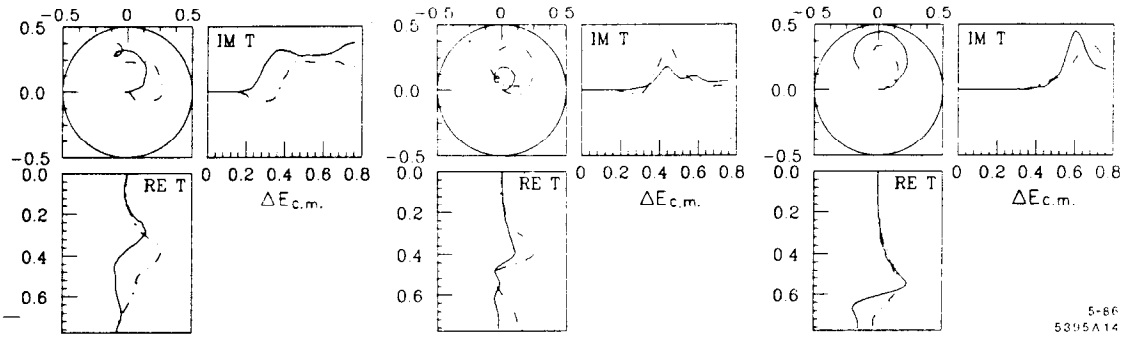

Fig. 13 (from Ref. 13). Test of Eq. (41). The left-hand side of (41), which refers to $\pi N \to \pi N$, and the right-hand side of (41), which refers to $\pi N \to \pi\Delta$, are depicted by solid and dashed lines, respectively.

7. Skyrmions and Vector Mesons

The notable success of the Skyrme model in describing both static and dynamic properties of baryons has lent credence to the chiral soliton picture of the nucleon. Of course, if this picture is at all sensible, we ought to expect that

the more realistic the theory of mesons that we start with, the more accurate our predictions of baryonic properties will be. In constructing a realistic theory, the most important modification to consider is the incorporation of additional low-lying mesons into the effective Lagrangian.

Work along these lines is just beginning. In the "ω-stabilized" Skyrme model of Adkins and Nappi,[26] one introduces a coupling $\omega_\mu B^\mu$ between the ω meson and the topological current of the theory. This coupling, which accounts for the decay $\omega \to 3\pi$, turns out to be sufficient to guarantee a stable soliton. Pleasingly, the static properties of the nucleon in this model constitute an improvement over the unadulterated Skyrme model. One can likewise construct stable solitons when the Lagrangian includes ρ-mesons, although the static properties of this model are as yet undetermined.[27] A recent model incorporating ω, ρ and A_1 mesons seems especially promising.[28]

In this Section we generalize the πN scattering formalism presented in Section 3 to the case when the skyrmion is coupled to an arbitrary number of different species of mesons. The processes we will focus on will be of the type

$$\phi B \longrightarrow \psi B'$$

where ϕ and ψ stand for generic mesons of arbitrary spin, isospin and parity,* and B and B' denote either a nucleon or a Δ. The treatment will be on a general level; we will not specify a Lagrangian. Nevertheless, as we shall see, the formalism implies the existence of nontrivial model-independent linear relations between these partial-wave scattering amplitudes, analogous to those of Section 4.

Our fundamental assumption will be that the effective meson theory admits a soliton solution which is a singlet under the simultaneous action $\mathbf{I}+\mathbf{J}$ of isospin and angular momentum. Such is the case in the usual Skyrme model, where the skyrmion is a hedgehog configuration (Eq. (5)). This can be thought of as the pion field's having acquired a spatially varying vacuum expectation value

$$< \pi^a(x) >= \frac{f_\pi}{2} F(r) \hat{x}_a \,. \tag{42}$$

In a more general Lagrangian, there is no reason for the skyrmion to confine itself entirely to the pion field. For example, in the model of Adkins and Nappi,[26,28] the (non-propagating) time component of the ω likewise acquires a

* In fact, they need not be mesons at all, but might, for instance, represent a quark interacting with a skyrmion in a "hybrid" model of quarks and pions.

VEV:

$$< \omega_0(x) >= G(r)\,, \quad < \omega_i(x) >= 0. \tag{43}$$

Similarly, in ρ-stabilized models,[27,28] the ρ field is characterized by

$$< \rho_0^a(x) >= 0\,, \quad < \rho_i^a(x) >= \epsilon_{ija}\hat{x}_j H(r)/r\,. \tag{44}$$

Note that Eqs. (43) and (44) also satisfy the fundamental assumption stated above.

Equations (42)-(44) generalize what in Section 3 we referred to as a skyrmion in its canonical (*i.e.*, unrotated) orientation. Of course, just as in the usual Skyrme model, one can use isospin invariance to construct a family of degenerate soliton solutions by rotating the canonical configuration through an angle $A \in SU(2)$:

$$\begin{aligned} < \pi^a(x) > &\longrightarrow \mathcal{D}^{(1)}(A)_{ab}\frac{f_\pi}{2}F(r)\hat{x}_b\,; \\ < \rho_i^a(x) > &\longrightarrow \mathcal{D}^{(1)}(A)_{ab}\epsilon_{ijb}\hat{x}_j H(r)/r\,. \end{aligned} \tag{45}$$

Nevertheless, let us forget for the moment about the existence of these degenerate configurations, and focus exclusively on the soliton in its canonical orientation.

We are thus (temporarily) interested in studying the two-point function $< \psi_j^b \phi_i^a >_0$ representing the simplified process

$$\phi U \longrightarrow \psi U,$$

where U stands for "unrotated skyrmion." The upper and lower indices on ϕ_i^a and ψ_j^b denote isospin and spin, respectively; the mesons will be assumed to be in representations $I_{\phi,\psi}$ of isospin and $S_{\phi,\psi}$ of spin. The nought on the propagator will remind us (as in Section 3) that the skyrmion is in its canonical orientation.

The key to our results is the observation that the vectorial sum

$$\mathbf{K} = \mathbf{S}_\phi + \mathbf{L} + \mathbf{I}_\phi \tag{46}$$

of the meson's angular momentum and isospin will be conserved in such a process. This conservation law, which is a direct consequence of our fundamental assumption, is the appropriate generalization of Eq. (9). As in Section 3, we can make the most of this symmetry by expanding the meson field in eigenstates of $\mathbf{K}^2$ and K_z, as follows: First, ϕ and ψ are expanded in spherical harmonics $|LM >$ and $|L'M' >$, respectively. Orbital angular momentum is then added

to isospin to form states $|\tilde{\mathbf{K}}^2\tilde{K}_z\mathbf{L}^2>$ and $|\tilde{\mathbf{K}}'^2\tilde{K}'_z\mathbf{L}'^2>$, where $\tilde{\mathbf{K}}=\mathbf{L}+\mathbf{I}_\phi$ and $\tilde{\mathbf{K}}'=\mathbf{L}'+\mathbf{I}_\psi$. This hybrid angular momentum is, in turn, added to the meson's spin to form states $|\mathbf{K}^2K_z\tilde{\mathbf{K}}^2\mathbf{L}^2>$ and $|\mathbf{K}^2K_z\tilde{\mathbf{K}}'^2\mathbf{L}'^2>$. We thus have:

$$\begin{aligned}<\psi_j^b(x')\phi_i^a(x)>_0 = &\sum_{LML'M'} Y_{L'M'}(\Omega')Y^*_{LM}(\Omega)\\ &\times\sum_{\tilde{K}\tilde{K}_z\tilde{K}'\tilde{K}'_z}<\mathbf{L}'\mathbf{I}_\psi|\tilde{\mathbf{K}}'><\tilde{\mathbf{K}}|\mathbf{L}\mathbf{I}_\phi>\sum_{KK_z}<\tilde{\mathbf{K}}'\mathbf{S}_\psi|\mathbf{K}><\mathbf{K}|\tilde{\mathbf{K}}\mathbf{S}_\phi>\\ &\times\mathcal{T}_{K\tilde{K}\tilde{K}'LL'},\end{aligned} \tag{47}$$

where $\mathcal{T}$ is the reduced amplitude for the process $\phi U\to\psi U$, and $<\tilde{\mathbf{K}}|\mathbf{L}\mathbf{I}_\phi>$ is shorthand for the Clebsch $<\tilde{K}\tilde{K}_zLI_\phi|LI_\phi Ma>$, *etc.* This is the appropriate analog of Eq. (11).

It is easy to generalize this formula to the case when the skyrmion, instead of being in its canonical orientation, has been rotated through an angle A, as in Eq. (45). By isospin invariance, the 2-point function simply becomes

$$<\psi_j^b\phi_i^a>_0\longrightarrow<\psi_j^b\phi_i^a>_A=\mathcal{D}^{(I_\psi)}(A)_{bd}<\psi_j^d\phi_i^c>_0\mathcal{D}^{(I_\phi)}(A)^\dagger_{ca}\,, \tag{48}$$

generalizing Eq. (13). Physical $\phi B\longrightarrow\psi B'$ scattering then requires that we fold in the initial and final baryon wavefunctions, exactly as in Eq. (14).

To compare with experiment, some further massaging is in order. We first restrict the incoming and outgoing mesons to orbital angular momenta L and L', respectively. The initial and final meson-baryon systems are then projected onto states $|I_{\rm tot}I_{{\rm tot}z}J_{\rm tot}J_{{\rm tot}z}S_{\rm tot}>$ and $|I'_{\rm tot}I'_{{\rm tot}z}J'_{\rm tot}J'_{{\rm tot}z}S'_{\rm tot}>$ of definite total isospin, angular momentum, and spin. Altogether, this projection leaves us with an expression for the propagator involving a product of 14 Clebsches! Fortunately, upon summation, our expression simplifies enormously, and we find:

$$<\psi\phi>_{\rm physical}=\delta_{I_{\rm tot}I'_{\rm tot}}\delta_{I_{{\rm tot}z}I'_{{\rm tot}z}}\delta_{J_{\rm tot}J'_{\rm tot}}\delta_{J_{{\rm tot}z}J'_{{\rm tot}z}}\sum_{K\tilde{K}\tilde{K}'}\eta\eta'\mathcal{T}_{K\tilde{K}\tilde{K}'LL'}. \tag{49}$$

Here η and η' are group-theoretic coefficients characterizing the entering and exiting channels, respectively; they are given in terms of $9j$-symbols by:

$$\eta=[(2K+1)(2\tilde{K}+1)(2R+1)(2S_{\rm tot}+1)]^{\frac{1}{2}}\begin{Bmatrix}L & I_\phi & \tilde{K}\\ S_{\rm tot} & R & S_\phi\\ J & I & K\end{Bmatrix} \tag{50a}$$

and

$$\eta' = [(2K+1)(2\widetilde{K}'+1)(2R'+1)(2S'_{\rm tot}+1)]^{\frac{1}{2}} \begin{Bmatrix} L' & I_\psi & \widetilde{K}' \\ S'_{\rm tot} & R' & S_\psi \\ J & I & K \end{Bmatrix} . \qquad (50b)$$

Note that conservation of isospin and angular momentum has emerged in the Kronecker-δ's of Eq. (49).

Equations (49) and (50) are the desired generalization of Eq. (18) to the case when the initial and/or final meson has arbitrary spin and isospin. Reassuringly, if one plugs $S_\phi = S_\psi = 0$ and $I_\phi = I_\psi = 1$ (*i.e.*, the quantum numbers of the pion) into (50), then the $9j$-symbols collapse into $6j$-symbols, and we recover Eq. (18). In the remainder of this Section, we shall concentrate on the model-independent predictions implied by Eq. (49) for the processes $\pi N \to \rho N$ and $\pi N \to \omega N$.

Let us denote the independent amplitudes for $\pi N \to \rho N$ by the notation $\mathbf{T}^{\pi N \rho N}_{LL',I_{\rm tot},J_{\rm tot},S_{\rm tot}}$. When $L' = L \pm 2$, Eq. (49) can be shown to imply a simple proportionality between the isospin-$\frac{1}{2}$ and the corresponding isospin-$\frac{3}{2}$ amplitudes:

$$\begin{aligned} \mathbf{T}^{\pi N\rho N}_{L,L+2,\frac{3}{2},L+\frac{1}{2},\frac{3}{2}} &= -\frac{1}{2}\mathbf{T}^{\pi N\rho N}_{L,L+2,\frac{1}{2},L+\frac{1}{2},\frac{3}{2}} ; \\ \mathbf{T}^{\pi N\rho N}_{L,L-2,\frac{3}{2},L-\frac{1}{2},\frac{3}{2}} &= -\frac{1}{2}\mathbf{T}^{\pi N\rho N}_{L,L-2,\frac{1}{2},L-\frac{1}{2},\frac{3}{2}} . \end{aligned} \qquad (51)$$

Similarly, for the more complicated case where $L' = L$, Eq. (49) implies that the four independent isospin-$\frac{3}{2}$ amplitudes for each value of L can be expressed as linear combinations of the four isospin-$\frac{1}{2}$ amplitudes. We find:

$$\begin{bmatrix} \mathbf{T}^{\pi N\rho N}_{LL\frac{3}{2},L-\frac{1}{2},\frac{1}{2}} \\ \mathbf{T}^{\pi N\rho N}_{LL\frac{3}{2},L+\frac{1}{2},\frac{1}{2}} \\ \mathbf{T}^{\pi N\rho N}_{LL\frac{3}{2},L-\frac{1}{2},\frac{3}{2}} \\ \mathbf{T}^{\pi N\rho N}_{LL\frac{3}{2},L+\frac{1}{2},\frac{3}{2}} \end{bmatrix} = \frac{1}{4\mathrm{L}+2} \begin{bmatrix} -\alpha^2 & -\beta^2 & -\beta\gamma & -\alpha^{-1}\beta^2\delta \\ -\alpha^2 & -\beta^2 & \alpha^2\beta^{-1}\gamma & \alpha\delta \\ -\beta\gamma & \beta\gamma & -2 & \alpha^{-1}\beta\gamma\delta \\ -\alpha\delta & \alpha\delta & \alpha\beta^{-1}\gamma\delta & 2 \end{bmatrix} \begin{bmatrix} \mathbf{T}^{\pi N\rho N}_{LL\frac{1}{2},L-\frac{1}{2},\frac{1}{2}} \\ \mathbf{T}^{\pi N\rho N}_{LL\frac{1}{2},L+\frac{1}{2},\frac{1}{2}} \\ \mathbf{T}^{\pi N\rho N}_{LL\frac{1}{2},L-\frac{1}{2},\frac{3}{2}} \\ \mathbf{T}^{\pi N\rho N}_{LL\frac{1}{2},L+\frac{1}{2},\frac{3}{2}} \end{bmatrix} \qquad (52)$$

with $\alpha = \sqrt{L}$, $\beta = \sqrt{L+1}$, $\gamma = \sqrt{2L-1}$, and $\delta = \sqrt{2L+3}$.

Figure 14 illustrates Eqs. (51) and (52) as applied to the experimental partial-wave $\pi N \to \rho N$ amplitudes, drawn from Ref. 22. The channels depicted are, unfortunately, the only ones for which sufficient experimental information is currently available for comparison. One should bear in mind that the curves do not represent the data directly, but result from a delicate, model-dependent

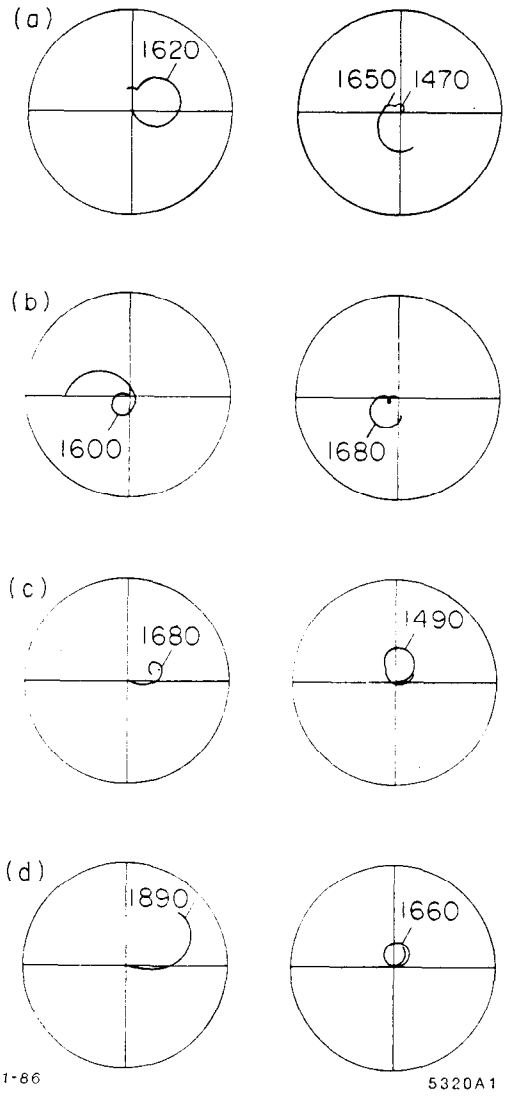

Fig. 14 (from Ref. 10). Comparison of experimental isospin-$\frac{3}{2}$ $\pi N \to \rho N$ amplitudes (left-hand column) with the appropriate multiple of the experimental isospin-$\frac{1}{2}$ amplitudes (right-hand column) to which they should correspond to leading order in $1/N$.

analysis of the $\pi\pi N$ final state. As such, they should not be taken as definitive.* Although the shapes of the curves in the left- and right-hand columns are not in particularly good correspondence, the agreement in the *signs* of the appreciably-coupled resonances (*i.e.*, whether the curve lies in the upper or lower half of the circle at a resonance energy) is completely nontrivial. This in itself can be regarded as quite promising—especially when contrasted to the fact that $SU(6)$ (in both its "unbroken" and "l-broken" versions) makes several incorrect (relative) sign predictions for the resonances shown.[22]

Of course, Eq. (49) implies similar model-independent linear relations that are straightforward to derive for such experimentally accessible processes as $\pi N \to \rho\Delta$, $\pi N \to fN$, and $\pi N \to \omega N$. For example, in the latter case, one can show:

$$\begin{aligned} &\mathbf{T}^{\pi N\omega N}_{LL\frac{1}{2},L-\frac{1}{2},\frac{1}{2}} - \mathbf{T}^{\pi N\omega N}_{LL\frac{1}{2},L+\frac{1}{2},\frac{1}{2}} \\ &\qquad = \sqrt{\frac{2L-1}{L+1}} \cdot \mathbf{T}^{\pi N\omega N}_{LL\frac{1}{2},L-\frac{1}{2},\frac{3}{2}} + \sqrt{\frac{2L+3}{L}} \cdot \mathbf{T}^{\pi N\omega N}_{LL\frac{1}{2},L+\frac{1}{2},\frac{3}{2}} \ . \end{aligned} \tag{53}$$

When reliable experimental low-energy partial-wave data for such processes become available, they will constitute further important tests of the chiral soliton approach to hadron physics.

8. Formalism for 3-Flavor Scattering

In this Section we extend the formalism for πN and $\pi\Delta$ scattering presented in Section 3 to the case of three light flavors. This will enable us to study processes of the form

$$\phi B \to \phi' B',$$

where ϕ and ϕ' are pseudoscalar-octet mesons and B and B' are $\frac{1}{2}^+$ octet or $\frac{3}{2}^+$ decuplet baryons. We shall work in the limit of *exact* $SU(3)_{\text{flavor}}$; the opposite limit, corresponding to $m_K \gg m_\pi$, has been studied in Ref. 6. The development in this Section closely parallels that of the 2-flavor case, presented in Section 3.

We shall again be focusing on Lagrangians such as Eq. (1) where now U is an element of $SU(3)$. In addition, the action must be augmented by the

* In particular, the large "tail" on the SD_{31} curve actually exceeds the unitarity bounds imposed by the elastic partial-wave amplitudes (*cf.* Fig. 3 of Ref. 22); similarly for the FP_{35}.

addition of the Wess-Zumino term

$$-\frac{iN}{240\pi^2}\int d^5x\epsilon^{ijklm}\,\mathrm{Tr}(U^\dagger\partial_i UU^\dagger\partial_j UU^\dagger\partial_k UU^\dagger\partial_l UU^\dagger\partial_m U) \tag{54}$$

which correctly reproduces the flavor-current anomalies of the strong interactions; here the integration is over the manifold $S^3\times D^2$ whose boundary is compactified space-time $S^3\times S^1$.[29]

As in the case of 2-flavor scattering, the key assumption is that the Lagrangian admits a hedgehog soliton solution U_0 that lives in the conventional $SU(2)_{\text{isospin}}$ subgroup of $SU(3)$, *viz* :

$$U_0=\exp\left\{iF(r)\sum_{i=1}^{3}\hat{\mathbf{r}}^i\lambda^i\right\}, \tag{55}$$

with λ^a, $a=1,...,8$, the Gell-Mann matrices. We shall refer to U_0 as a 3-flavor skyrmion in its *canonical* orientation.*

Of course, other orientations of the skyrmion are possible. In fact, by virtue of the assumed $SU(3)_{\text{flavor}}$ invariance of the Lagrangian, one can construct a family of degenerate solitons simply by taking

$$U_A=AU_0A^{-1},\quad A\in SU(3). \tag{56}$$

However, as before, it is convenient to forget at first about the existence of these degenerate configurations, and concentrate on the simplified problem of mesons scattering from U_0. This entails letting

$$U_0\longrightarrow\exp\left\{iF(r)\sum_{i=1}^{3}\hat{\mathbf{r}}^i\lambda^i+\frac{2i}{f_\pi}\sum_{a=1}^{8}\phi^a\lambda^a\right\} \tag{57}$$

and expanding the Lagrangian to quadratic order in the ϕ's. In particular, the Wess-Zumino term makes a contribution

$$\frac{iN}{4\pi^2}\int d^4x\frac{F'\sin^2F}{F^2r^2}(1-\cos F)(K^-\dot{K}^+ +\overline{K}^0\dot{K}^0) \tag{58}$$

to the quadratic action.†

---

* The results of this Section would be unaffected if the η field had a radially-dependent expectation-value as well, although this is not the case for the particular example of Skyrme's Lagrangian.

† This contrasts with the baryon-number-zero sector of the theory, in which the Wess-Zumino term first contributes to five-meson processes.[30,29]

What will the resulting quadratic Lagrangian look like? Thanks to the hedgehog structure of the skyrmion, it will consist of a sum of terms in which all isospin and spatial indices have been contracted together in all possible ways to form singlets under the "hybrid" angular momentum $\mathbf{K}$, which is the vectorial sum of isospin and angular momentum. Also, since the skyrmion (55) commutes with λ^8, the Lagrangian will embody hypercharge conservation. Consequently, kaons will be coupled only to kaons, and antikaons to antikaons. There will be $\pi\pi$ and $\eta\eta$ couplings as well, but $\pi\eta$ terms are forbidden by G-parity. In other words, the T-matrix $\mathbf{T}^{ba}$ characterizing the process

$$\phi^a + \text{canonical skyrmion} \longrightarrow \phi^b + \text{canonical skyrmion},$$

which is *a priori* an 8×8 matrix in the flavor-space of pseudoscalar-octet mesons, actually block-diagonalizes into a 3×3, a 1×1, and two 2×2 pieces, corresponding to π, η, K and $\overline{K}$ scattering, respectively.

We have not yet made full use of the $\mathbf{K}$ symmetry of the canonical skyrmion. To do so, we first expand ϕ^a and ϕ^b in spherical harmonics Y_{LM} and $Y_{L'M'}$, with primes as always denoting final-state quantities. These orbital angular momenta are, in turn, added to the mesons' isospin $\mathbf{I}^a$ and $\mathbf{I}^b$ by familiar Clebsch-Gordanry to form states $|\mathbf{K}^2 K_z \mathbf{L}^2 \mathbf{I}^{a2}>$ and $|\mathbf{K}'^2 K'_z \mathbf{L}'^2 \mathbf{I}^{b2}>$. The $\mathbf{K}$ symmetry of the canonically-oriented skyrmion then implies $\mathbf{K}^2 = \mathbf{K}'^2$ and $K_z = K'_z$; likewise, thanks to the block-diagonal nature of $\mathbf{T}^{ba}$, we must have $I^a = I^b$. In contrast, L and L' will not necessarily be equal, but can differ by two. Scattering in these $\mathbf{K}$-channels will then be described by the reduced amplitudes $\mathcal{T}^{\{I,Y\}}_{KL'L}$, where $\{I,Y\}$ runs over the values $\{1,0\}$, $\{0,0\}$, and $\{\frac{1}{2},\pm 1\}$. In equations, the T-matrix will thus be given by:

$$\begin{aligned}\mathbf{T}^{ba} \;=\; & \delta_{I^a I^b}\delta_{Y^a Y^b} \sum_{LML'M'} <\phi^b(x')|L'M'><LM|\phi^a(x)> \\ & \times \sum_{KK_z} <L'I^bM'I^b_z|KK_z><KK_z|LI^aMI^a_z>\, \mathcal{T}^{\{I^aY^a\}}_{KL'L}\end{aligned} \tag{59}$$

where $\{I^a, I^a_z, Y^a\}$ and $\{I^b, I^b_z, Y^b\}$ are the $SU(3)$ quantum numbers of the incoming and outgoing meson, respectively.

This formula is easily generalized to account for the scattering of a meson, not from a canonically-oriented skyrmion U_0, but rather from a rotated skyrmion U_A as defined by Eq. (56). The prescription is simply

$$\mathbf{T}^{ba} \longrightarrow \sum_{cd} \mathcal{D}^{(8)}(A)_{bd}\, \mathbf{T}^{dc}\, \mathcal{D}^{(8)}(A)^\dagger_{ca} \tag{60}$$

with $\mathcal{D}^{(8)}(A)$ the adjoint representation of A. Armed with Eqs. (59) and (60), we are finally prepared to tackle the scattering of a meson off a physical baryon,

which, as in the 2-flavor case, is characterized by a *superposition* of U_A's for all values of $A \in SU(3)$, weighted by appropriately-constructed wavefunctions $\chi(A)$. The physical T-matrix is then given by:

$$\int_{SU(3)} dA\ \chi^\dagger_{\rm final}(A) \sum_{cd} \mathcal{D}^{(8)}(A)_{bd}\, \mathbf{T}^{dc}\, \mathcal{D}^{(8)}(A)^\dagger_{ca} \chi_{\rm initial}(A)\ . \tag{61}$$

The final ingredient that we need is an explicit expression for the baryon wavefunctions $\chi(A)$ describing a baryon with spin, isospin and hypercharge quantum numbers $\{s, s_z, i, i_z, Y\}$. Unfortunately, the 3-flavor wavefunctions given by Guadagnini,[31] which are often used in the literature, are characterized by nonstandard transformation properties under isospin and angular momentum. The correct wavefunctions are, instead,

$$\chi(A) = \frac{i}{\pi}\sqrt{\frac{\dim R}{2}}[\mathcal{D}^R(A)^\dagger]_{\alpha,\beta} \cdot (-1)^{s-s_z} \tag{62}$$

where $\alpha = \{s, -s_z, 1\}$, $\beta = \{i, i_z, Y\}$ and R denotes the $SU(3)_{\rm flavor}$ representation of the baryon.*

As in the 2-flavor case,[8] the integration over A can be carried out in closed form, thanks to some standard identities. The resulting expression simplifies greatly if, in addition, we project the initial and final meson-baryon systems onto states of definite total angular momentum $\mathbf{J}$ and $\mathbf{J}'$, and total $SU(3)_{\rm flavor}$ defined by quantum numbers† $\{R_{\rm tot}, \gamma, I_{\rm tot}, I_{z\rm tot}, Y_{\rm tot}\}$. (The latter projection is accomplished with the help of an $SU(3)$ Clebsch-Gordan coefficient

$$\langle R_1 i_1 i_{z1} Y_1; R_2 i_2 i_{z2} Y_2 | R_{\rm tot}\gamma I_{\rm tot} I_{z\rm tot} Y_{\rm tot}\rangle$$

which can be factored conveniently into the product

$$\langle i_1 i_2 i_{z1} i_{z2} | I_{\rm tot} I_{z\rm tot}\rangle \cdot \left(\begin{array}{cc|c} R_1 & R_2 & R_{\rm tot}\gamma \\ i_1 Y_1 & i_2 Y_2 & I_{\rm tot}\ Y_{\rm tot} \end{array}\right)$$

of an $SU(2)$ Clebsch-Gordan coefficient with a so-called isoscalar factor.[33]) We

---

* See, for example, Manohar.[32] The fact that the "left-handed hypercharge" is unity is a nontrivial quantization condition arising from consideration of the Wess-Zumino term.[31] Our normalization in (62) is such that $\int_{SU(3)} dA = 2\pi^2$.

† Here γ is a largely redundant index whose only real purpose is to distinguish between degenerate representations that can occur in the product of two $SU(3)$ representations, as for example the $\mathbf{8}_{\rm sym}$ and $\mathbf{8}_{\rm antisym}$ in $\mathbf{8} \times \mathbf{8}$.[33] As can be seen in Eq. (3), it is *not* in general conserved, even for exact $SU(3)_{\rm flavor}$. To understand this, one need only consider the nonvanishing $\mathbf{8}_{\rm antisym} \leftrightarrow \mathbf{8}_{\rm sym}$ coupling $\mathrm{Tr}(\{\overline{B}, \Phi\}[B, \Phi])$ between the baryon octet B and the meson octet Φ.

find, after some massaging:

$$\mathbf{T}(\{LsRR_{\rm tot}\gamma I_{\rm tot}I_{z\rm tot}Y_{\rm tot}\mathbf{J}\}\to\{L's'R'R'_{\rm tot}\gamma' I'_{\rm tot}I'_{z\rm tot}Y'_{\rm tot}\mathbf{J}'\}) \quad =$$

$$\delta_{R_{\rm tot}R'_{\rm tot}}\delta_{I_{\rm tot}I'_{\rm tot}}\ \delta_{I_{z\rm tot}I'_{z\rm tot}}\ \delta_{Y_{\rm tot}Y'_{\rm tot}}\ \delta_{JJ'}\delta_{J_zJ'_z}\quad\times$$

$$(-1)^{s'-s}\frac{\sqrt{\dim R\cdot\dim R'}}{\dim R_{\rm tot}}\sum_{\{IY\}}\sum_i\sum_K(2i+1)(2K+1)\begin{Bmatrix}KiJ\\ s'L'I\end{Bmatrix}\begin{Bmatrix}KiJ\\ sLI\end{Bmatrix}$$

$$\times\quad\left(\begin{array}{cc|cc}R_{\rm tot}\gamma' & & R' & \mathbf{8}\\ i,1+Y & & s'1 & IY\end{array}\right)\left(\begin{array}{cc|cc}R & \mathbf{8} & & R_{\rm tot}\gamma\\ s1 & IY & & i,1+Y\end{array}\right)\mathcal{T}^{\{IY\}}_{KL'L}\,. \tag{63}$$

The long string of Kronecker δ's expresses the reassuring fact that total angular momentum and $SU(3)_{\rm flavor}$ are conserved in the scattering process. The index K assumes integral values when $\{IY\}=\{1,0\}$ or $\{0,0\}$ and odd-half-integral values when $\{IY\}=\{\frac{1}{2},\pm1\}$, while the index i assumes odd-half-integral and integral values, respectively, in these cases. In addition, these sums are constrained by the various triangle inequalities implicit in the two $6j$ symbols (*cf.* Fig. 3), as a consequence of which we find the following contributing reduced amplitudes for physical processes:

$\underline{\phi B\to\phi' B' \text{ with } L'=L:}$

the eight reduced amplitudes $\{\mathcal{T}^{\{1,0\}}_{L\pm1,LL},\ \mathcal{T}^{\{1,0\}}_{LLL},\ \mathcal{T}^{\{0,0\}}_{LLL},\ \mathcal{T}^{\{\frac{1}{2},1\}}_{L\pm\frac{1}{2},LL},\ \mathcal{T}^{\{\frac{1}{2},-1\}}_{L\pm\frac{1}{2},LL}\}$ all contribute;

$\underline{\phi B\to\phi' B' \text{ with } L'=L\pm2:}$

only $\mathcal{T}^{\{1,0\}}_{KL'L}$, $K=(L+L')/2$, contributes.

Of course, for most physical processes, one is interested in a *superposition* of pure $SU(3)_{\rm flavor}$ representations. As an illustration, consider the case $\overline{K}N\to\pi\Sigma$ in the isospin-1 channel. With the help of the table of isoscalar factors given in Ref. 33, the initial and final states can be written as

$$|\Psi>_{\rm in}=\frac{1}{\sqrt{5}}|\mathbf{27}>+\frac{1}{\sqrt{6}}|\overline{\mathbf{10}}>-\frac{1}{\sqrt{6}}|\mathbf{10}>-\frac{\sqrt{30}}{10}|\mathbf{8}_{\rm sym}>+\frac{1}{\sqrt{6}}|\mathbf{8}_{\rm antisym}>$$

and

$$_{\rm out}<\Psi|=-\frac{1}{\sqrt{6}}<\overline{\mathbf{10}}|+\frac{1}{\sqrt{6}}<\mathbf{10}|+\frac{\sqrt{6}}{3}<\mathbf{8}_{\rm antisym}|\,.$$

The amplitude for this process is thus given by

$$
\begin{aligned}
{}_{\text{out}}\!<\Psi|\Psi>_{\text{in}} = & -\frac{1}{6}<\overline{\mathbf{10}}|\overline{\mathbf{10}}> -\frac{1}{6}<\mathbf{10}|\mathbf{10}> \\
& -\frac{1}{\sqrt{5}}<\mathbf{8}_{\text{antisym}}|\mathbf{8}_{\text{sym}}> +\frac{1}{3}<\mathbf{8}_{\text{antisym}}|\mathbf{8}_{\text{antisym}}> .
\end{aligned}
$$

Each term in this expression can, in turn, be expressed in terms of reduced amplitudes using Eq. (63).

Note that the derivation of (63) is independent of the particular Lagrangian that we started from, apart from the requirement that it admit a hedgehog soliton as in Eq. (55).

It is important to check whether the generally successful model-independent relations for $\pi N \to \pi N$ and $\pi N \to \pi\Delta$ analyzed in Section 4 survive the incorporation of strangeness. *A priori*, there is no cause for optimism on this score, for the following reason. In the 2-flavor approach, the four physical πN amplitudes for each $L > 0$ (*i.e.*, $J = L \pm \frac{1}{2}$ and $I = \frac{1}{2}, \frac{3}{2}$) are expressed through Eq. (19) as superpositions of only three reduced amplitudes. Consequently, at least one nontrivial relation between physical amplitudes is guaranteed for each value of L (in fact, there turned out to be two). In contrast, in the 3-flavor approach, these same four amplitudes are linear combinations of *eight* reduced amplitudes. It should therefore come as a surprise that *all of the linear relations except for Eq. (23) survive virtually unscathed in the 3-flavor formalism.* The only modification consists of small correction terms in Eqs. (20) and (21) related to the presence of the Wess-Zumino term (see Section 7 of Ref. 13 for details).

9. The 3-Flavor Skyrme Model

This Section applies Eq. (63) to the specific case of the 3-flavor Skyrme model, whose action is given by the sum of Eqs. (29) and (54), with $U \in SU(3)$. A comprehensive analysis of all πN, KN and $\overline{K}N$ processes in the 3-flavor Skyrme model *vs.* experiment is to be found in Ref. 13; here we can give only a smattering of results.

πN Scattering

Figures 9 and 12 given earlier in Section 5 display both the 2- and 3-flavor Skyrme-model predictions for the nonstrange processes $\pi N \to \pi N$ and $\pi N \to \pi\Delta$, juxtaposed with experiment. In general, the 3-flavor graphs constitute an improvement over their 2-flavor counterparts. This is primarily a matter

of *scale*: the 3-flavor formalism allows for inelastic channels such as $K\Sigma$ which are not present in the 2-flavor approach, and which consequently serve to shrink the size of the curves.

Interestingly, the 3-flavor Skyrme model can be shown to contain secondary resonances in the F_{15} and F_{37} channels that are in plausible correspondence with the tentatively observed states at 1882 and 2350 MeV, respectively.[12] Other than this, however, the 2- and 3-flavor Skyrme models yield virtually identical spectra of nucleon and Δ resonances, summarized in Fig. 11.

In general, there is reasonable agreement between the 3-flavor Skyrme model and experiment for πN processes involving strangeness, *viz.*, $\pi N \to K\Sigma$, $\pi N \to K\Lambda$, and $\pi N \to \eta N$. (It should be mentioned that the experimental situation here is much less reliable than for $\pi N \to \pi N$ and $\pi N \to \pi\Delta$.) Figure 15 presents the results for $\pi N \to K\Lambda$. Here, the most noticeable feature of the model is the sign alternation characterizing the plots; this "down-up" pattern appears to be present in Nature as well, albeit in a less clearcut manner. Not surprisingly, there is poor agreement between the model and experiment in the S-wave channel, just as for $\pi N \to \pi N$.

KN Scattering

One can also use the 3-flavor scattering formalism to study KN scattering. KN processes occupy a special role from the point of view of the quark model, since resonances in these channels (unlike $\overline{K}N$) cannot correspond to qqq, but rather $qqqq\overline{q}$ states. Not surprisingly, in Nature, the majority of amplitudes show no hint of a resonance, and are in fact repulsive (that is, curve clockwise). The existence of *any* such resonances is still an open question, with the most recent analyses favoring such a state in the D_{03} channel, and probably in several others as well.

Figure 16 illustrates elastic KN scattering in the Skyrme model juxtaposed with the results of the two latest partial-wave analyses.[35,36] The overall degree of agreement between the model and experiment is poor. This should not come as a surprise, for the following reason. It turns out that the 3-flavor Skyrme model with $N = 3$ contains as rotational excitations of the canonical hedgehog soliton, Eq. (55), an infinite tower of baryon multiplets *beyond* the usual spin-$\frac{1}{2}$ octet and spin-$\frac{3}{2}$ decuplet.[31] This tower includes, in particular, a spin-$\frac{1}{2}$ $\overline{\mathbf{10}}$ and spin-$\frac{1}{2}$ and spin-$\frac{3}{2}$ $\mathbf{27}$'s. Each of these multiplets would naturally be expected to have excitations of higher angular momentum, just as the usual octet and decuplet have; such states would manifest themselves as resonances in KN scattering. In short, there is nothing exotic about KN processes in the Skyrme model; this is confirmed by the multitude of obviously resonant Skyrme-model amplitudes in Fig. 16.

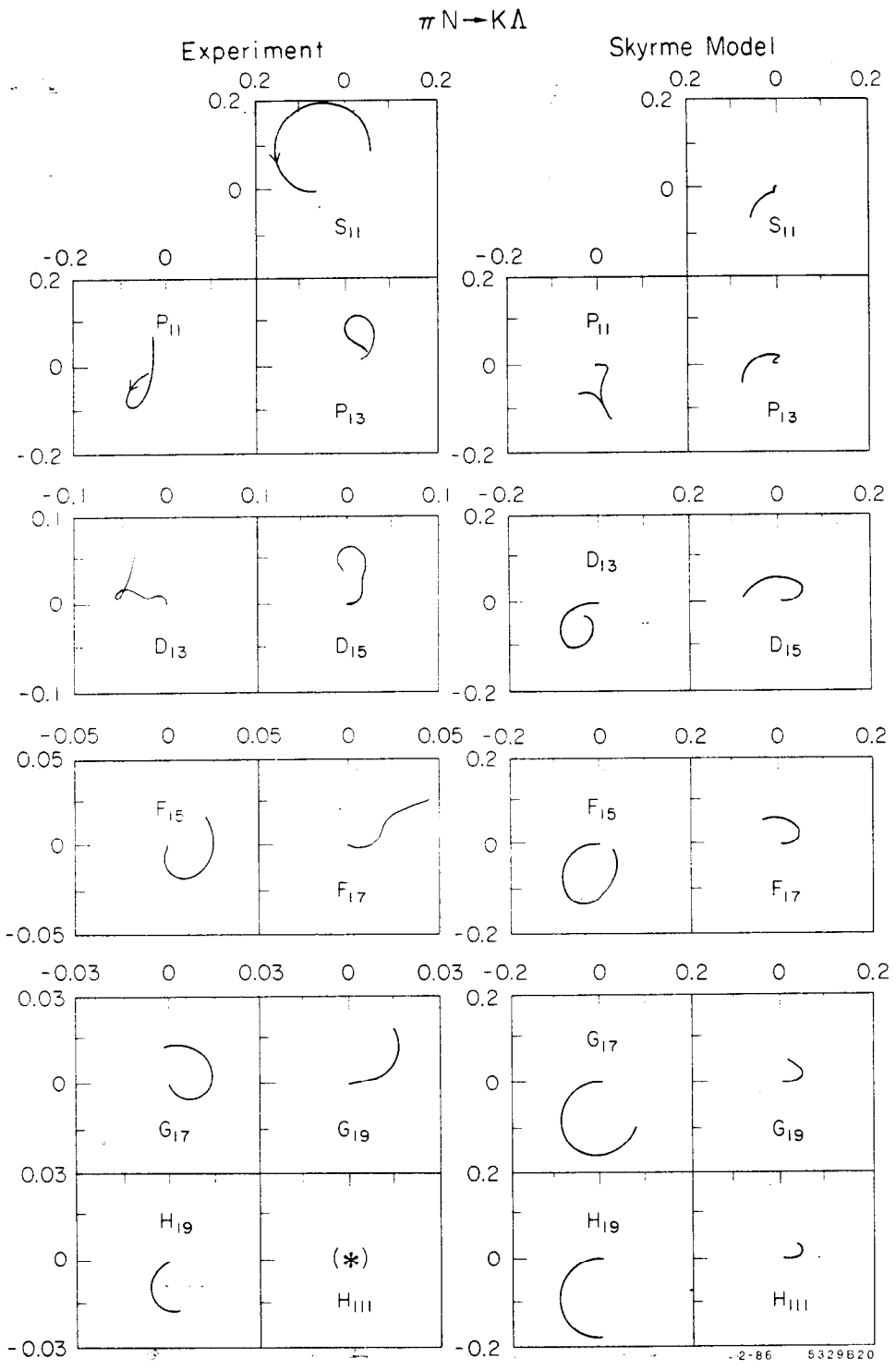

Fig. 15 (from Ref. 13). $\pi N \to K\Lambda$: comparison between the Skyrme model and experiment.[34] Channels are labeled by $L_{2I,2J}$. Note that experimental and Skyrme-model plots are shown on different scales.

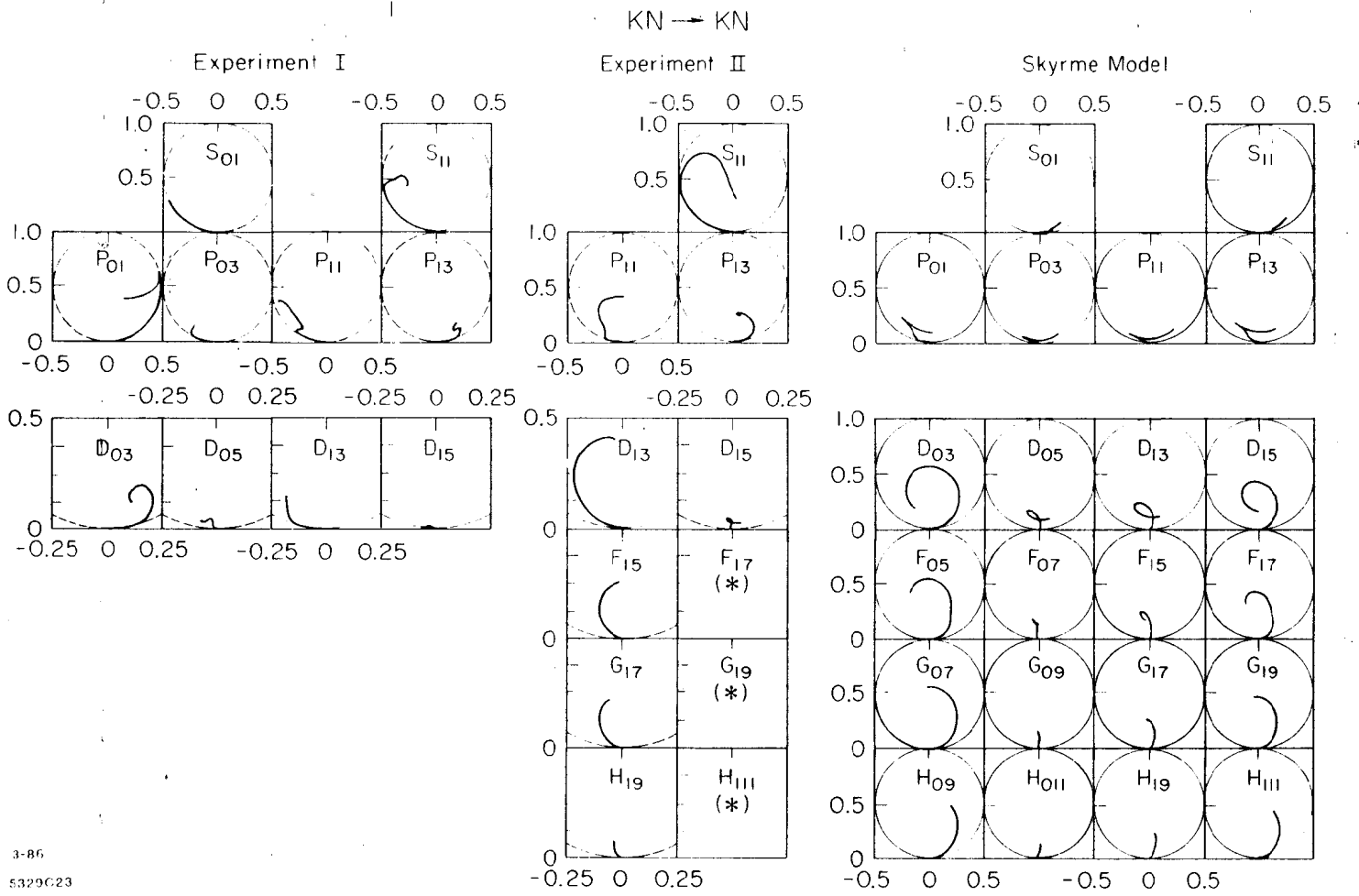

Fig. 16 (from Ref. 13). $KN \to KN$: comparison between the Skyrme model and two experimental solutions: "Experiment I" from Ref. 36; and "Experiment II" from Ref. 35. Channels are labeled by $L_{I,2J}$. Note that experimental and Skyrme-model plots for $L \geq 2$ are shown on different scales.

It is instructive to consider an analogous situation involving the 2-flavor Skyrme model. It is well known that this model contains states with $I = J = \frac{1}{2}, \frac{3}{2}, \frac{5}{2}, \frac{7}{2}, \ldots$ that emerge as rotational excitations of the hedgehog.[3] The two lowest-lying multiplets are naturally identified with the nucleons and Δ's, respectively, while the states with $I = J \geq \frac{5}{2}$ are traditionally labeled "artifacts of the model" and swept under the rug. Thankfully, isospin conservation forbids these states from appearing in the s-channel of πN scattering, so that they do not really cause a problem.* However, one can consider the *gedanken* experiment of $\pi^+\Delta^{++}$ scattering, which is pure isospin-$\frac{5}{2}$. From the quark point of view, this is an exotic process just like KN scattering, and we would expect to see a high proportion of repulsive amplitudes. In contrast, in the skyrmion approach, there is nothing exotic about this channel, since isospin-$\frac{5}{2}$ states exist; indeed, nearly all the Skyrme model graphs for $\pi^+\Delta^{++} \to \pi^+\Delta^{++}$ evince the usual resonant behavior.

The moral is that the skyrmion approach can hardly be expected to yield accurate information about KN scattering, as these processes directly probe those states that one would prefer to dismiss as unphysical artifacts of the model. This having been said, it is interesting to speculate about whether those exotic states that *do* seem to be present in Nature reflect in any way the "skyrminess" of the nucleon. We offer the following cautious observations:

1. Although the four P-wave Skyrme-model amplitudes appear to be repulsive, close inspection reveals that the P_{01} and P_{13} amplitudes actually curve anticlockwise before the cusps. Therefore, they might be interpreted as very weak resonances superimposed on a strongly repulsive background. It is interesting to note that these are the same two P-wave amplitudes that curve anticlockwise in Nature.

2. The D_{03} channel is the most prominent of the D-wave curves in the Skyrme model, and it is the most plausibly resonant D-wave channel in Nature as well.

3. Interestingly, there appears to be some unexpected resemblance in both the P- and D-wave sectors between the four $KN \to KN$ experimental amplitudes and their $\pi N \to \pi N$ counterparts (compare "Experiment I" in Fig. 16 to Fig. 9). In particular, in the P waves, the first and fourth amplitudes for both processes curve anticlockwise, while the second and third curve clockwise. Likewise, the D waves are characterized by a pattern of "decreasingly resonant behavior" across the four graphs in each process. Consequently, it is conceivable that the same $1/N$ corrections that are expected to improve the agreement in

* Note that an isospin-$\frac{5}{2}$ baryon $B_{\frac{5}{2}}$ *can* be produced in the Skyrme model in the process $\pi N \to \pi B_{\frac{5}{2}}$ and is therefore required for unitarity.

these waves between the Skyrme model and experiment for $\pi N \to \pi N$ will do likewise for $KN \to KN$.

4. Lastly, we have come to expect reasonable agreement between the Skyrme model and experiment in the F, G and H waves. It is unfortunate that the only such channels for which experimental $KN \to KN$ amplitudes have been presented, namely the F_{15}, G_{17} and H_{19}, are predicted by the Skyrme model to be small and rather featureless (Fig. 16). A much more critical test of whether the model has anything relevant to say about KN scattering would be the appearance of resonances in the F_{05}, G_{07} and H_{09} channels. An analysis of these channels can be expected in the not-too-distant future.*

$\overline{K}N$ Scattering

Finally, the Skyrme model gives mixed results in describing $\overline{K}N$ scattering. On the level of individual graphs, the model works less well on the whole for $\overline{K}N$ than for πN scattering. Nevertheless, in certain important respects, the agreement is quite pleasing. Most notably, for the processes $\overline{K}N \to \overline{K}N$ and $\overline{K}N \to \pi\Sigma$, depicted in Figs. 17 and 18, respectively, the model successfully reproduces a pattern reminiscent of $\pi N \to \pi N$ that characterizes the four independent experimental amplitudes for each value of L: specifically, in the model as in Nature, the P_{01}, D_{03}, F_{05} and G_{07} amplitudes travel significantly further through the unitarity circle than do their counterparts. Not surprisingly, this "big-small-small-small" pattern finds the same sort of natural group-theoretical explanation in the context of 3-flavor chiral soliton models as we invoked in Section 6 for the big-small-small-big pattern in 2-flavor models; the interested reader is referred to Section 6 of Ref. 13 for full details.

All in all, despite areas of deep disagreement with experiment, such as "exotic" KN processes, and S- and P-wave scattering in general, we consider the overall degree of accord obtained from such a simple model as Skyrme's to be powerful evidence for the validity of the chiral soliton approach to baryon physics.

* R. A. Arndt, private communication.

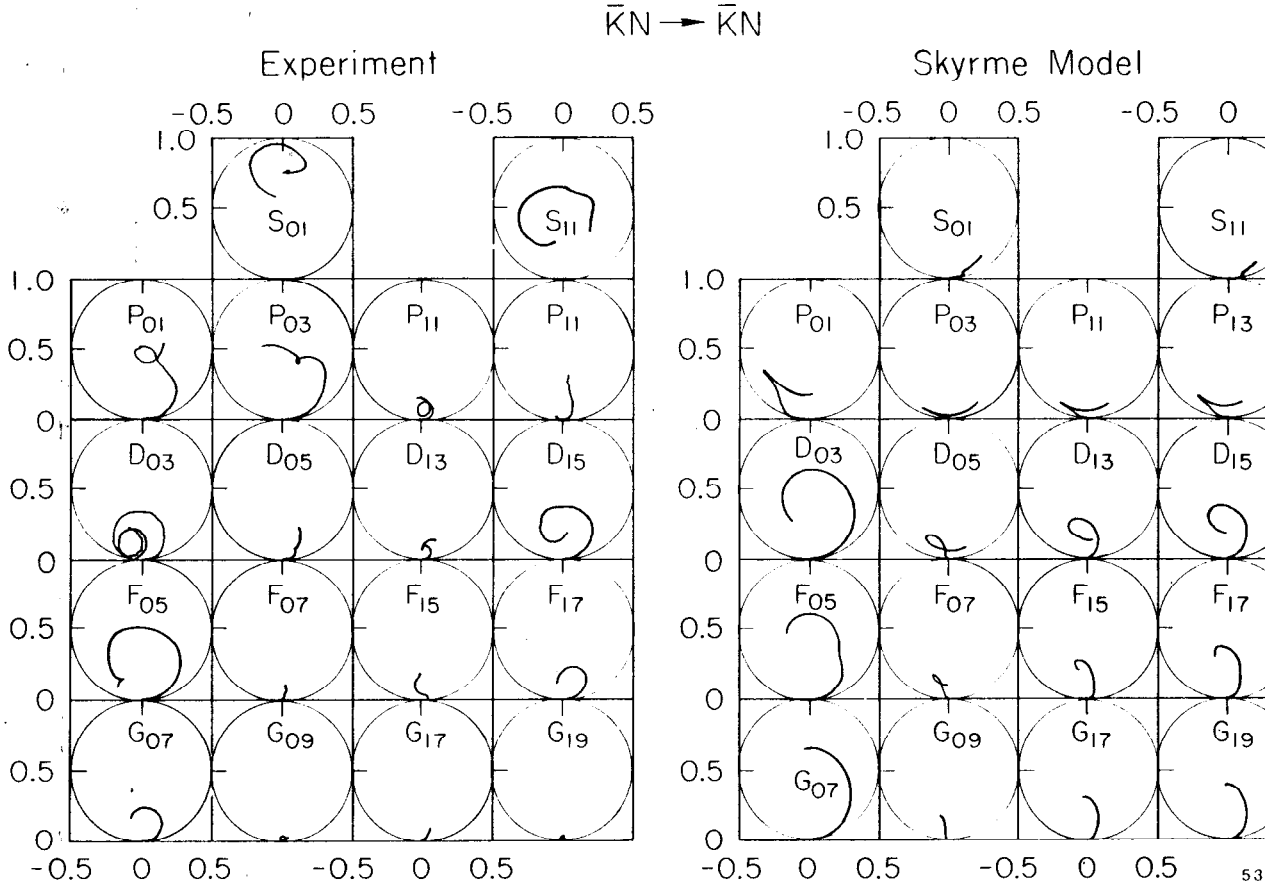

Fig. 17 (from Ref. 13). $\overline{K}N \to \overline{K}N$ **: comparison between the Skyrme model and experiment.**[38] **Channels are labeled by** $L_{I,2J}$.

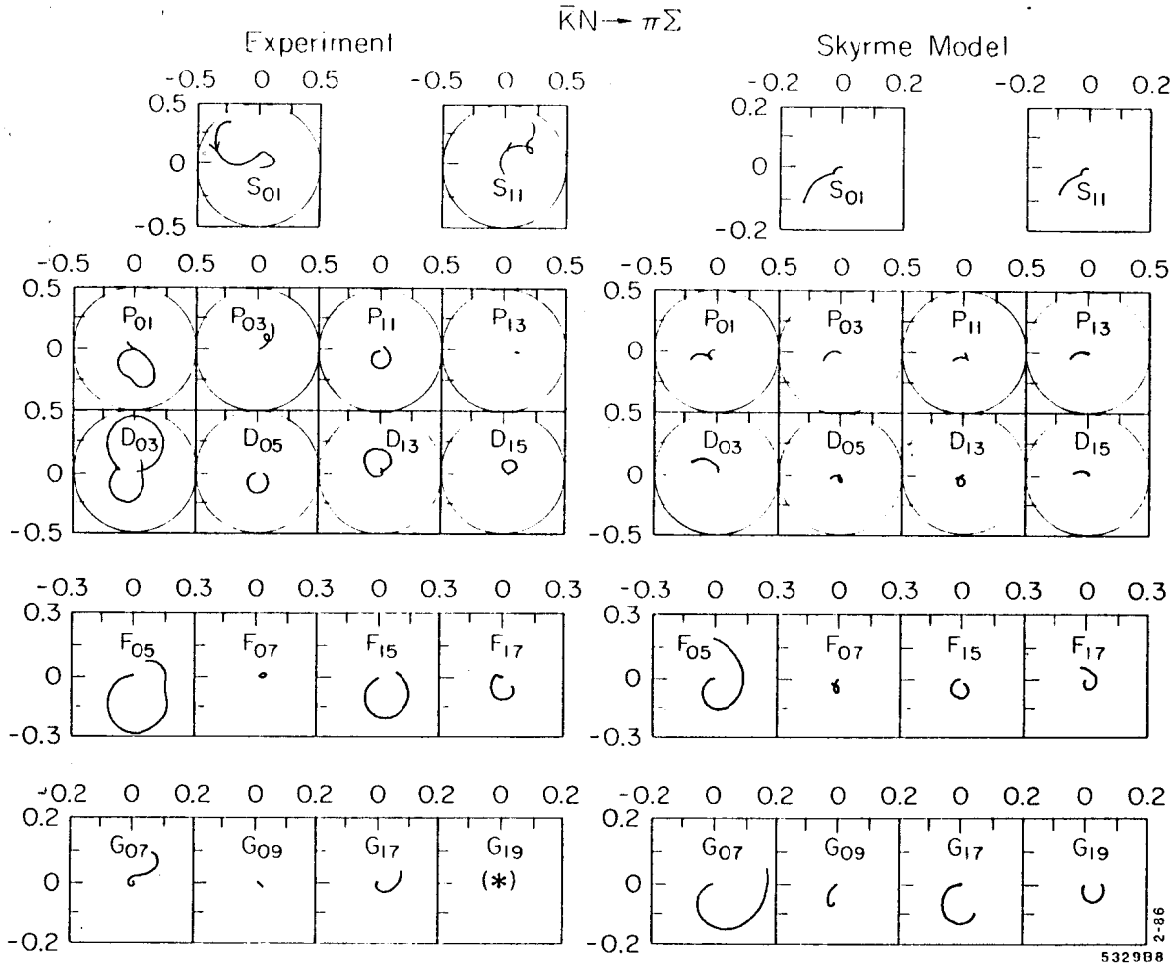

Fig. 18 (from Ref. 13). $\overline{K}N \to \pi\Sigma$: comparison between the Skyrme model and experiment.[38] Channels are labeled by $L_{I,2J}$. Note that the experimental and Skyrmé-model plots for $L = 0$ are shown on different scales.

10. References

1. T. H. R. Skyrme *Proc. Roy. Soc.* **A260** (1961) 127.
2. T. H. R. Skyrme, *Nucl. Phys.* **31** (1962) 556.
3. G. Adkins, C. Nappi, and E. Witten, *Nucl. Phys.* **B228**, 552 (1983).
4. H. Schnitzer, *Phys. Lett.* **139B**, 217 (1984); *Nucl. Phys.* **B261** (1985) 546.
5. I. Zahed, U.-G. Meissner, and U. B. Kaulfuss, *Nucl. Phys.* **A426**, 525 (1984); J. D. Breit and C. R. Nappi, *Phys. Rev. Lett.* **53**, 889 (1984); J. D. Breit, *Phys. Lett.* **153B** (1985) 300; C. Hajduk and B. Schwesinger, *Phys. Lett.* **140B** (1984) 172; J. Dey and J. Le Tourneux, in *Solitons in Nuclear and Elementary Particle Physics* (conference proceedings), Lewes, 1984; K. F. Liu, J. S. Zhang and G. R. E. Black, *Phys. Rev.* **D30** (1984) 2015; A. Parmentola, *Phys. Rev.* **D30** (1984) 685; L. C. Biedenharn, Y. Dothan, and M. Tarlini, *Phys. Rev.* **D31** (1985) 649.
6. C. G. Callan and I. Klebanov, *Nucl. Phys.* **B262** (1985) 365.
7. M. P. Mattis and M. Karliner, *Phys. Rev.* **D31** (1985) 2833.
8. M. P. Mattis and M. Peskin, *Phys. Rev.* **D32** (1985) 58.
9. M. Peskin, *Pion-skyrmion scattering: collective coordinates at work*, SLAC-PUB 3703, in *Recent Developments in Quantum Field Theory*, J. Ambjørn, B. J. Durhuus and J. L. Petersen, *eds.*, Elsevier, 1985.
10. M. P. Mattis, *Phys. Rev. Lett.* **56** (1986) 1103.
11. M. P. Mattis, *Aspects of Meson-Skyrmion Scattering*, SLAC-PUB. 3795, September 1985, in S. Brodsky and E. Moniz, eds., Proceedings of the 1985 ITP Workshop on Nuclear Chromodynamics, World Scientific Press.
12. M. Karliner and M. P. Mattis, *Phys. Rev. Lett.* **56** (1986) 428.
13. M. Karliner and M. P. Mattis, *πN, KN and $\overline{K}N$ Scattering: Skyrme Model vs. Experiment*, SLAC-PUB-3901, 1986.
14. H. Walliser and G. Eckart, *Nucl. Phys.* **A429**, 514 (1984).
15. A. Hayashi, G. Eckart, G. Holzwarth, and H. Walliser, *Phys. Lett.* **147B**, 5 (1984).
16. S. Coleman, J. Wess, B. Zumino, *Phys. Rev.* **177** (1969) 2239; C. Callan, S. Coleman, J. Wess, B. Zumino, *ibid.* 2247.
17. S. Weinberg, *Phys. Rev. Lett.* **17**, 168 (1966).
18. E. Witten *Nucl. Phys.* **B160** 57 (1979).
19. G. 't Hooft, *Nucl. Phys.* **B72** (1974) 461; *Nucl. Phys.* **B75** (1974) 461.

20. G. Höhler, F. Kaiser, R. Koch, and E. Pietarinen, *Handbook of Pion-Nucleon Scattering* (Fachinformationszentrum, Karlsruhe, 1979), Physik Daten No. 12-7. Reproduced in Review of Particle Properties, *Rev. Mod. Phys.* **56**, part II (1984).

21. M. Uehara and H. Kondo, *πN Scattering lengths in the skyrmion model,* Saga Univ. preprint, SAGA-HE-19, Dec. 1985.

22. D. M. Manley, R. A. Arndt, Y. Goradia, and V. L. Teplitz, *Phys. Rev.* **D30**, 904 (1984).

23. M. Messiah, *Quantum Mechanics*, Amsterdam, North Holland, 1961.

24. R. E. Cutkosky *et al.*, in *Baryon* 1980 (conference proceedings), ed. N. Isgur; reproduced in Review of Particle Properties, *op. cit.*

25. R. A. Arndt, J. M. Ford and L. D. Roper, *Phys. Rev.* **D32** (1985) 1085.

26. Adkins and Nappi, *Phys. Lett.* **137B**, 251 (1984).

27. T. Fujiwara *et al.*, *Prog. Theor. Phys.* **74**, 128 (1985); Y. Igarashi *et al.*, *Nucl. Phys.* **B259**, 721 (1985). Note, however, that the attack on Ref. 26 given here is in error.

28. U.-G. Meissner and I. Zahed, *Phys. Rev. Lett.* **56** (1986) 1035.

29. E. Witten *Nucl. Phys.* **B223** (1983) 422; *ibid.* 433.

30. J. Wess and B. Zumino, *Phys. Lett.* **37B** (1971) 95.

31. E. Guadagnini, *Nucl. Phys.* **B236** (1984) 35.

32. A. Manohar, *Nucl. Phys.* **B248** 19 (1984).

33. J. J. deSwart, *Rev. Mod. Phys.* **35** (1963) 916; reprinted in M. Gell-Mann and Y. Ne'eman, *The Eightfold Way*, New York 1964, p. 120.

34. K. W. Bell *et al.*, *Nucl. Phys.* **B222** (1983) 389.

35. R. A. Arndt and L. D. Roper, *Phys. Rev.* **D31** (1985) 2230.

36. K. Hashimoto, *Phys. Rev.* **C29** (1984) 1377.

37. K. Nakajima *et al.*, *Phys. Lett.* **112B**, 80 (1982).

38. G. P. Gopal *et al.*, *Nucl. Phys.* **B119** (1977) 362. Reproduced in Review of Particle Properties, *op. cit.*